Society for the Promotion of Science (A: 24249019, B: 25293085 25293235, C: 24591500, 23590363), the Takeda Science Foundation, the fund for Creation of Innovation Centers for Advanced Interdisciplinary Research Areas Program in the Project for Developing Innovation Systems, the Strategic Research Program for Brain Sciences (11105137), and a Grant-in-Aid for Scientific Research on Innovative Areas (transcription cycle, exploring molecular basis for brain diseases based on personal genomics) from the Ministry of Education, Culture, Sports, Science and Technology of Japan (12024421, 25129705).

DISCLOSURE

M. Kato is funded by research grants from the Ministry of Health, Labour and Welfare of Japan, and a Grant-in-Aid for Scientific Research (C) from the Japan Society for the Promotion of Science. H. Saitsu is funded by a Grant-in-Aid for Scientific Research (B) from the Japan Society for the Promotion of Science, and the Takeda Science Foundation. Y. Murakami is funded by a Grant-in-Aid for Scientific Research (C) from the Japan Society for the Promotion of Science, the Takeda Science Foundation, a Grant-in-Aid for Scientific Research on Innovative Areas (exploring molecular basis for brain diseases based on personal genomics) from the Ministry of Education, Culture, Sports, Science and Technology of Japan. K. Kikuchi, S. Watanabe, M. Iai, K. Miya, R. Matsuura, R. Takayama, C. Ohba, M. Nakashima, and Y. Tsurusaki report no disclosures relevant to the manuscript. N. Miyake is funded by research grants from the Ministry of Health, Labour and Welfare of Japan, a Grant-in-Aid for Scientific Research (B) from the Japan Society for the Promotion of Science, and the Takeda Science Foundation. S. Hamano, H. Osaka, and K. Hayasaka report no disclosures relevant to the manuscript. T. Kinoshita is supported by a Grant-in-Aid for Scientific Research (A) from the Japan Society for the Promotion of Science. N. Matsumoto is supported by grants from the Ministry of Health, Labour and Welfare of Japan, a Grant-in-Aid for Scientific Research (A) from the Japan Society for the Promotion of Science, the Takeda Science Foundation, the fund for Creation of Innovation Centers for Advanced Interdisciplinary Research Areas Program in the Project for Developing Innovation Systems, the Strategic Research Program for Brain Sciences, a Grant-in-Aid for Scientific Research on Innovative Areas (transcription cycle) from the Ministry of Education, Culture, Sports, Science and Technology of Japan. Go to Neurology.org for full disclosures.

Received November 7, 2013. Accepted in final form February 7, 2014.

REFERENCES

1. Kato M, Saitoh S, Kamei A, et al. A longer polyalanine expansion mutation in the *ARX* gene causes early infantile epileptic encephalopathy with suppression-burst pattern (Ohtahara syndrome). Am J Hum Genet 2007;81:361–366.
2. Saitsu H, Kato M, Mizuguchi T, et al. De novo mutations in the gene encoding STXBP1 (MUNC18-1) cause early infantile epileptic encephalopathy. Nat Genet 2008;40: 782–788.
3. Saitsu H, Kato M, Osaka H, et al. *CASK* aberrations in male patients with Ohtahara syndrome and cerebellar hypoplasia. Epilepsia 2012;53:1441–1449.
4. Kato M, Yamagata T, Kubota M, et al. Clinical spectrum of early onset epileptic encephalopathies caused by *KCNQ2* mutation. Epilepsia 2013;54:1282–1287.
5. Nakamura K, Kato M, Osaka H, et al. Clinical spectrum of *SCN2A* mutations expanding to Ohtahara syndrome. Neurology 2013;81:992–998.
6. Kato M. A new paradigm for West syndrome based on molecular and cell biology. Epilepsy Res 2006;70(suppl 1): S87–S95.
7. Saitsu H, Tohyama J, Kumada T, et al. Dominant-negative mutations in alpha-II spectrin cause West syndrome with severe cerebral hypomyelination, spastic quadriplegia, and developmental delay. Am J Hum Genet 2010;86:881–891.
8. Kurian MA, Meyer E, Vassallo G, et al. Phospholipase C beta 1 deficiency is associated with early-onset epileptic encephalopathy. Brain 2010;133:2964–2970.
9. Almeida AM, Murakami Y, Layton DM, et al. Hypomorphic promoter mutation in *PIGM* causes inherited glycosylphosphatidylinositol deficiency. Nat Med 2006;12: 846–851.
10. Hansen L, Tawamie H, Murakami Y, et al. Hypomorphic mutations in *PGAP2*, encoding a GPI-anchor-remodeling protein, cause autosomal-recessive intellectual disability. Am J Hum Genet 2013;92:575–583.
11. Johnston JJ, Gropman AL, Sapp JC, et al. The phenotype of a germline mutation in *PIGA*: the gene somatically mutated in paroxysmal nocturnal hemoglobinuria. Am J Hum Genet 2012;90:295–300.
12. Krawitz PM, Murakami Y, Hecht J, et al. Mutations in *PIGO*, a member of the GPI-anchor-synthesis pathway, cause hyperphosphatasia with mental retardation. Am J Hum Genet 2012;91:146–151.
13. Krawitz PM, Schweiger MR, Rodelsperger C, et al. Identity-by-descent filtering of exome sequence data identifies *PIGV* mutations in hyperphosphatasia mental retardation syndrome. Nat Genet 2010;42:827–829.
14. Kvarnung M, Nilsson D, Lindstrand A, et al. A novel intellectual disability syndrome caused by GPI anchor deficiency due to homozygous mutations in *PIGT*. J Med Genet 2013;50:521–528.
15. Maydan G, Noyman I, Har-Zahav A, et al. Multiple congenital anomalies-hypotonia-seizures syndrome is caused by a mutation in *PIGN*. J Med Genet 2011;48: 383–389.
16. Ng BG, Hackmann K, Jones MA, et al. Mutations in the glycosylphosphatidylinositol gene *PIGL* cause CHIME syndrome. Am J Hum Genet 2012;90:685–688.
17. DePristo MA, Banks E, Poplin R, et al. A framework for variation discovery and genotyping using next-generation DNA sequencing data. Nat Genet 2011; 43:491–498.
18. Saitsu H, Nishimura T, Muramatsu K, et al. De novo mutations in the autophagy gene *WDR45* cause static encephalopathy of childhood with neurodegeneration in adulthood. Nat Genet 2013;45:445–449.
19. Wang K, Li M, Hakonarson H. ANNOVAR: functional annotation of genetic variants from high-throughput sequencing data. Nucleic Acids Res 2010;38:e164.
20. Molinari F, Raas-Rothschild A, Rio M, et al. Impaired mitochondrial glutamate transport in autosomal recessive neonatal myoclonic epilepsy. Am J Hum Genet 2005;76: 334–339.
21. Nozaki M, Ohishi K, Yamada N, Kinoshita T, Nagy A, Takeda J. Developmental abnormalities of glycosylphosphatidylinositol-anchor-deficient embryos revealed by Cre/loxP system. Lab Invest 1999;79:293–299.
22. Watanabe S, Murayama A, Haginoya K, et al. Schinzel-Giedion syndrome: a further cause of early myoclonic encephalopathy and vacuolating myelinopathy. Brain Dev 2012;34:151–155.
23. Barone R, Aiello C, Race V, et al. DPM2-CDG: a muscular dystrophy-dystroglycanopathy syndrome with severe epilepsy. Ann Neurol 2012;72:550–558.
24. Yang AC, Ng BG, Moore SA, et al. Congenital disorder of glycosylation due to *DPM1* mutations presenting with dystroglycanopathy-type congenital muscular dystrophy. Mol Genet Metab 2013;110:345–351.

25. Sener RN. Diffusion magnetic resonance imaging patterns in metabolic and toxic brain disorders. Acta Radiol 2004; 45:561–570.
26. Kuki I, Takahashi Y, Okazaki S, et al. Vitamin B6-responsive epilepsy due to inherited GPI deficiency. Neurology 2013; 81:1467–1469.
27. Aicardi J. Aicardi syndrome. Brain Dev 2005;27: 164–171.
28. Lehman AM, McFadden D, Pugash D, Sangha K, Gibson WT, Patel MS. Schinzel-Giedion syndrome: report of splenopancreatic fusion and proposed diagnostic criteria. Am J Med Genet A 2008;146A: 1299–1306.
29. Hoischen A, van Bon BW, Gilissen C, et al. De novo mutations of *SETBP1* cause Schinzel-Giedion syndrome. Nat Genet 2010;42:483–485.
30. Kranz C, Denecke J, Lehrman MA, et al. A mutation in the human *MPDU1* gene causes congenital disorder of glycosylation type If (CDG-If). J Clin Invest 2001;108:1613–1619.
31. Almeida AM, Murakami Y, Baker A, et al. Targeted therapy for inherited GPI deficiency. N Engl J Med 2007;356: 1641–1647.

PLOS | GENETICS

Null Mutation in PGAP1 Impairing Gpi-Anchor Maturation in Patients with Intellectual Disability and Encephalopathy

Yoshiko Murakami[1]*, Hasan Tawamie[2], Yusuke Maeda[1], Christian Büttner[2], Rebecca Buchert[2], Farah Radwan[2], Stefanie Schaffer[3], Heinrich Sticht[4], Michael Aigner[3], André Reis[2], Taroh Kinoshita[1], Rami Abou Jamra[2]*

1 Research Institute for Microbial Diseases and WPI Immunology Frontier Research Center, Osaka University, Suita, Osaka, Japan, **2** Institute of Human Genetics, Friedrich-Alexander-Universität Erlangen-Nürnberg, Erlangen, Germany, **3** Department of Internal Medicine 5, Hematology and Oncology, University of Erlangen-Nürnberg, Erlangen, Germany, **4** Institute of Biochemistry, Friedrich-Alexander-Universität Erlangen-Nürnberg, Erlangen, Germany

Abstract

Many eukaryotic cell-surface proteins are anchored to the membrane via glycosylphosphatidylinositol (GPI). There are at least 26 genes involved in biosynthesis and remodeling of GPI anchors. Hypomorphic coding mutations in seven of these genes have been reported to cause decreased expression of GPI anchored proteins (GPI-APs) on the cell surface and to cause autosomal-recessive forms of intellectual disability (ARID). We performed homozygosity mapping and exome sequencing in a family with encephalopathy and non-specific ARID and identified a homozygous 3 bp deletion (p.Leu197del) in the GPI remodeling gene *PGAP1*. *PGAP1* was not described in association with a human phenotype before. PGAP1 is a deacylase that removes an acyl-chain from the inositol of GPI anchors in the endoplasmic reticulum immediately after attachment of GPI to proteins. In silico prediction and molecular modeling strongly suggested a pathogenic effect of the identified deletion. The expression levels of GPI-APs on B lymphoblastoid cells derived from an affected person were normal. However, when those cells were incubated with phosphatidylinositol-specific phospholipase C (PI-PLC), GPI-APs were cleaved and released from B lymphoblastoid cells from healthy individuals whereas GPI-APs on the cells from the affected person were totally resistant. Transfection with wild type *PGAP1* cDNA restored the PI-PLC sensitivity. These results indicate that GPI-APs were expressed with abnormal GPI structure due to a null mutation in the remodeling gene *PGAP1*. Our results add *PGAP1* to the growing list of GPI abnormalities and indicate that not only the cell surface expression levels of GPI-APs but also the fine structure of GPI-anchors is important for the normal neurological development.

Citation: Murakami Y, Tawamie H, Maeda Y, Büttner C, Buchert R, et al. (2014) Null Mutation in PGAP1 Impairing Gpi-Anchor Maturation in Patients with Intellectual Disability and Encephalopathy. PLoS Genet 10(5): e1004320. doi:10.1371/journal.pgen.1004320

Editor: Stefan Mundlos, Max Planck Institute for Molecular Genetics, Germany

Received October 24, 2013; **Accepted** March 7, 2014; **Published** May 1, 2014

Funding: This study was supported by the German Intellectual disability Network (MRNET) through a grant from the German Ministry of Research and Education to AR (01GS08160 and 01GR0804-4), by the Deutsche Forschungsgemeinschaft (DFG) through a grant to RAJ (AB393/2-1), by the Deutscher Akademischer Austauschdienst (DAAD) through a scholarship to HT, by Deutsche Forschungsgemeinschaft and Friedrich-Alexander-Universität Erlangen-Nürnberg (FAU) within the funding programe Open Access Publishing, by grants from the Ministry of Education, Culture, Sports, Science, and Technology of Japan (a Grant-in-Aid for Scientific Research C 23590363 and a Grant-in-Aid for Scientific Research on Innovative Areas, Exploring molecular basis for brain diseases based on personal genomics 25129705), and from the Takeda Science Foundation. The funders had no role in study design, data collection and analysis, decision to publish, or preparation of the manuscript.

Competing Interests: The authors have declared that no competing interests exist.

* E-mail: yoshiko@biken.osaka-u.ac.jp (YM); rami.aboujamra@uk-erlangen.de (RAJ)

Introduction

Many eukaryotic cell-surface proteins with various functions are anchored to the membrane via glycosylphosphatidylinositol (GPI) [1–3]. After biosynthesis in the endoplasmic reticulum (ER), GPI-anchors are transferred to the proteins by the GPI transamidase and the structure of the GPI-anchor is then remodeled, which is critical for sorting, regulating and trafficking of the GPI anchored proteins (GPI-APs) [3]. This remodeling starts in the ER by eliminating the acyl-chain linked to the inositol in the GPI-anchor by PGAP1 [4], then a side-chain of ethanolamine-phosphate on the second mannose of the GPI-anchor is removed by MPPE1 (PGAP5) [5]. GPI-APs are then transported from the ER to the plasma membrane through the Golgi apparatus, where further remodeling by PGAP3 and PGAP2 takes place [6,7]. Germline mutations in eight genes that are involved in the GPI-anchor biosynthesis and remodeling have been described (Table 1) [8–22]. The mutations in all of those, *PIGA*, *PIGL*, *PIGM*, *PIGV*, *PIGN*, *PIGO*, *PIGT* and *PGAP2*, are hypomorphic and lead to partially decreased cell surface expression of various GPI-APs, thus causing a wide phenotypic spectrum ranging from syndromic disorders with various malformations to non-specific forms of intellectual disability. The reported mutations in genes of early steps of the GPI-anchor synthesis such as *PIGA* (MIM 311770), *PIGL* (MIM 605947), and *PIGM* (MIM *610273), or in a gene involved in GPI transfer to proteins such as *PIGT* (MIM *610272) are supposed to result in a degradation of precursor non-GPI-anchored proteins by ER associated degradation, whereas mutations in genes that are involved in later steps of the pathway, such as *PIGV* (MIM *610274), *PIGO* (MIM *614730), and *PGAP2* (MIM *615187)

Author Summary

Glycosylphosphatidylinositols (GPI) are glycolipid anchors that anchor various proteins to the cell surface. At least 26 genes are involved in biosynthesis and modification of the GPI anchors. Recently, mutations in eight of those genes have been described. Although those mutations do not fully abolish the functions of encoded enzymes, they lead to a decreased expression of surface GPI-anchored proteins and to different forms of intellectual disability. Here we report a mutation in *PGAP1* that encodes a protein that modifies the GPI anchor. We found that the mutation leads to a full loss of PGAP1 enzyme activity, but that the patient cells still express normal levels of surface GPI-anchored proteins. However, the GPI anchors have an abnormal lipid structure that is resistant to cleavage by phosphatidylinositol-specific phospholipase C. Our results add *PGAP1* to the growing list of GPI abnormalities that cause intellectual disability and indicate that the fine structure of GPI-anchors is also important for a normal neurological development.

result in partial secretion of non-GPI-anchored proteins such as alkaline phosphatase (in case of *PIGV* or *PIGO* deficiency) [23] or of proteins bearing cleaved GPI-anchor (in case of *PGAP2* deficiency), and are therefore characterized by hyperphosphatasia. Here we report on the identification of a mutation in *PGAP1* that encodes the GPI inositol-deacylase [4]. This leads to a new type of GPI-anchor deficiency manifesting non-specific autosomal recessive intellectual disability (ARID), in which cell surface levels of GPI-APs are not affected whereas the structure of GPI moiety is abnormal.

Results

Clinical manifestations

We undertook clinical characterization, mapping [24] and exome sequencing in a large cohort of families with non-specific ARID. We identified the *PGAP1* mutation in the Syrian family MR079. The parents in family MR079 are the first-degree cousins and the family has one healthy girl and two affected children that carry the mutation in a homozygous status. The affected girl (III-2) was 4 years and 5 months old and the affected boy (III-3) was 2 years and 9 months old at the time of examination (Figure 1). Pregnancy, delivery, and birth parameters of both children were unremarkable. In the neonatal period, III-2 was hypotonic and III-3 was a floppy baby. Motor development was delayed; III-2 could sit at age of 18 months and at age of $4^{5/12}$ years first tried to walk independently. At age of $2^{9/12}$, III-3 could only roll from back to stomach and back. Both children did not finish potty training and were still partially fed with milk bottles. Both children have a developmental delay and severe intellectual disability with an estimated IQ below 35. III-2 could only babble a few syllables. While III-2 had major and absence epilepsy, III-3 did not yet have seizures. Sleeping patterns of both children were normal. They showed some stereotypic movements such as hitting on their own mouth and some washing movements of the hands. Both children seemed to see and hear properly, but specific tests could not be done. Brain CT scan of III-2 at age of one year revealed pronounced brain atrophy. At the time of examination, III-2 was 96 cm tall (25^{th} percentile) with a head circumference of 46 cm (2 cm below the 5^{th} percentile). III-3 was also of normal height and had a head circumference of 47 cm (1.5 cm below the 5^{th} percentile). Their parents had head circumferences of 52 and 53 cm, also in the lower percentiles. Both children have large ears and a flattened nasal root. G-banding, cytogenetic examination and genome wide copy number variants analyses were unremarkable. We did not have information on the levels of alkaline phosphatase and it was not possible to obtain blood probes retrospectively.

Exome sequencing revealed a homozygous mutation in *PGAP1*

Autozygosity mapping [24] in family MR079 led to the identification of six candidate regions of a total length of 64 Mb. Subsequently, exome sequencing using DNA from individual III-3 was performed as described in former studies [21,25] resulting in an average coverage of 53.28. 66% of the target sequences were covered with a depth of at least 20×, and 80.51% were covered with a depth of at least 5×. A total of 42,352 SNVs and 2,529 indels were identified. 342 SNVs and 64 indels were neither annotated, nor reported in 1000Genomes and Exome Variant Server, nor in in-house controls, and may affect the protein sequence (non-synonymous, splicing, or UTR). Of those, only two, in *PGAP1* and *SLC40A*, were located in a candidate region, conserved, and predicted to be pathogenic by *in silico* programs. To exclude further candidate mutations, we repeated the exome sequencing using DNAs of both affected siblings. We enriched the exome using a PCR based targeting method (Ion AmpliSeq Exome Kit) and sequenced on the Ion Proton. The average coverage of III-3 and III-2 was 149.6× and 94.6×, respectively. 91.1% and 85.0% of the target sequences were covered with a depth of at least 20×, 96.3% and 93.4% with a depth of at least 5×, respectively. A total of 49,455 and 47,693 SNVs as well as 3,343 and 3,167 indels were identified. When applying the above mentioned filtering steps, we were by both affected children once again left with the variants in *PGAP1* and *SLC40A*. Since mutations in *SLC40A* cause hemochromatosis of type 4 and have no effect on cognition (MIM 606069) [26,27], we focused on the variant in *PGAP1*, NM_024989.3:c.589_591delCTT, NP_079265.2:p.Leu197-del. Genotyping the variant in *PGAP1* in 372 healthy Syrian adults using Sanger sequencing revealed no further carriers. Taking the minor allele frequency of 0 in the Exome Sequencing Project (ESP) data set and in our control sample of 372 healthy Syrian individuals, it seems that the mutation has prevalence far less than 0.001.

Molecular modeling using the GeneSilico fold recognition metaserver [28] and Modeler9.9 [29] using the closest related hydrolase (PDB code: 3LP5) as template highlighted the detrimental effect of the deletion of leucine 197 on the structure of PGAP1. Leucine 197 is located in the central strand of a β-sheet and is oriented towards the hydrophobic core of the enzyme where it forms multiple stabilizing interactions with the adjacent helices (Figure 2A, B). Deletion of this amino acid would place Ile198 at the position originally occupied by Leu197 (Figure 2C). The Cβ-branched side-chain of isoleucine cannot be accommodated at this sequence position resulting in several clashes with adjacent amino acids (Leu184, Ile194) of the hydrophobic core (Figure 2C). This will disrupt the packing of the hydrophobic core and consequently of the entire β-sheet topology, thus leading to a loss of tertiary structure and enzymatic activity.

We then ran large scale homozygosity mapping using PLINK in our sample of over 100 consanguineous families [24] and over 600 sporadic cases of ID [30] and identified 7 index patients, 2 from consanguineous families with multiple affected children and 5 from outbreed families with single affected patients, that are homozygous at the *PGAP1*. Sequencing all seven individuals using Sanger did not reveal any mutations in *PGAP1*.

Table 1. Overview of identified mutations in the GPI synthesis pathway and the associated symptoms.

Gene (RefSeq)	Phenotypes	Families	Mutations	References
PIGA (NM_002641.3)	Multiple congenital anomalies involving cleft palate, neonatal seizures, central nervous system structural malformations, intellectual disability	3	homo[1] p.R412* homo p.Leu110del homo p.Pro93Leu	[9,10,11]
PIGL (NM_004278.3)	Coloboma, congenital heart disease, ichthyosiform dermatosis, intellectual disability, ear anomalies	5	comp het[2] p.Leu167Pro & p.Leu92Phefs*15 comp het p.Leu167Pro & p.Gln218* homo p.Leu167Pro comp het p.Leu167Pro & c.427-1G>A (Splice defect) comp het p.Leu167Pro & p.del17p12-p11.2	[19]
PIGM (NM_145167.2)	Portal and hepatic vein thrombosis in early childhood and seizures, no intellectual disability	2	promoter GC-BOX	[8]
PIGV (NM_017837.3)	Intellectual disability, characteristic face, seizures, brachytelephalangy, hyperphosphatasia,	14	homo p.Leu302Pro homo p.Ala341Glu comp het p.Ala341Glu & p.Leu59Arg comp het p.Ala341Glu & p.Cys18Tyr comp het p.Ala341Glu p.Arg469* comp het p.Ala341Glu & p.His385Pro homo p.Gly256Lys comp het p.Ala341Glu & p.Ala341Val comp het p.Ala341Glu & p.Cys156Tyr comp het p.Pro165Gln & p.Cys156Tyr	[13,14]
PIGN (NM_012327.5)	Multiple congenital anomalies, hypotonia, seizures, intellectual disability	2	homo p.Arg709Gln comp het p.Ser270Pro & c.963G>A (Splice defect)	[17,18]
PIGO (NM_032634.3)	Intellectual disability, recognizable facial characteristics, seizures, brachytelephalangy, hyperphosphatasia	4	comp het p.Leu957Phe & c.3069+5G>A(Splice defect) comp het p.Thr788Hisfs*5 & p.Leu957Phe comp het p. Arg119trp & p. Ala834fs*129 comp het p.Gln430* & p.Thr130Asn	[12,15,16]
PIGT (NM_015937)	Intellectual disability, hypotonia, characteristic facial features, seizures, and further skeletal, endocrine, and ophthalmologic findings, hypophosphatasia	1	homo p.Thr183Pro	[20]
PGAP1 (NM_024989.3)	Intellectual disability, major and absence epilepsy in 1 sibling, brain atrophy on CT scan	1	homo p.Leu197del	This study
PGAP2 (NM_001256240.1)	Severe intellectual disability, absence seizures, hyperphosphatasia	3	homo p.Tyr99Cys homo p.Arg77Pro comp het p.Arg16Trp & p.Thr160Ile	[21,22]

1: homozygous,
2: compound-heterozygous.
doi:10.1371/journal.pgen.1004320.t001

We then screened the exome variant server for functional variants in *PGAP1*. 149 variants are reported in this gene, of those 44 were coding or at splice sites. All of those are extremely rare (0.0077%–0.569%, i. e. 1–74 alleles out of ca. 13000 alleles). Based on the conservation of the variants and the prediction of *in silico* programs (Table S1), we roughly estimate that a maximum of 48 individuals may carry a mutation in *PGAP1* (carrier rate of 48/6500 = 0.0073) and that the prevalence of the disease would be about 13 per million. If we take more conservative *in silico* prediction numbers, the prevalence of the disease would be 7 per million inhabitants (Table S1). The two most frequent variants in the ESP data were p.Lys111Glu and p.Gln585Glu and were observed in a heterozygous form 15 and 74 times out of 12992 and 12932 alleles, respectively. Both sites are well conserved in the mammalian. Molecular modeling showed that the most common variant Gln585Glu is located outside of catalytic active domains and it was not possible to make a prediction for this variant. Lys111Glu is at the C terminus of a helix of the deacylase domain. The charging pattern of the helix is highly conserved so that we expect that the change from Lys to Glu would change the charge of the protein and destabilize the helix.

Flow cytometry of B-lymphoblastoid cell lines

To determine effects of p.Leu197del alteration on cellular GPI-APs, we investigated the surface expression of GPI-APs on B-lymphoblastoid cell lines (LCLs) derived from the homozygous

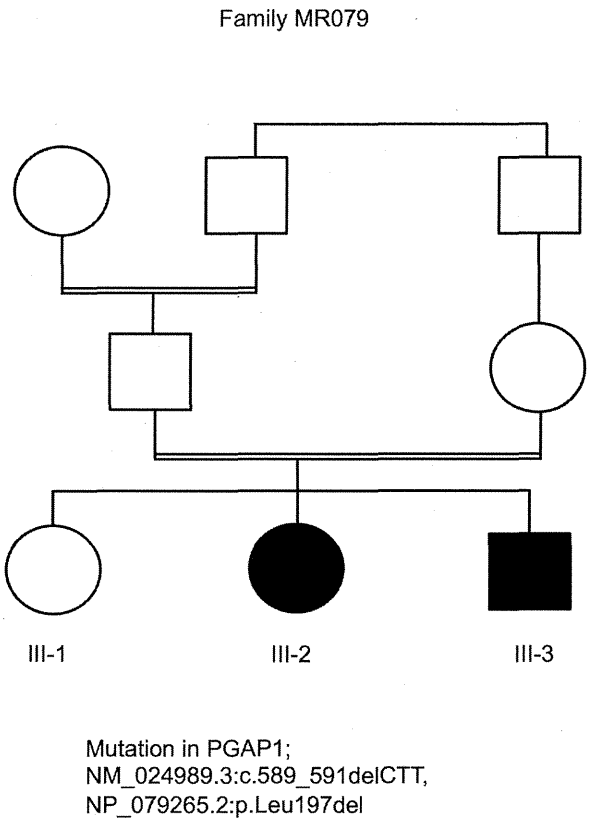

Figure 1. Pedigree of family MR079 and a PGAP1 mutation.
doi:10.1371/journal.pgen.1004320.g001

individual III-3 (−/−), 2 heterozygous parents (+/−), and the healthy sister (+/+) (Figure 3), as well as 6 healthy volunteers with a confirmed wild type genotype (data not shown). Using flow cytometry analysis, the respective surface expressions of CD59, CD55/DAF, and CD48 were quantified. Surface expression of these GPI-APs on LCLs from an affected person, other family members or healthy volunteers showed no significant difference, indicating that the *PGAP1* mutation did not affect the surface expression levels of various GPI-APs (Figure 3A, dotted lines). The surface expression of the GPI anchor itself was quantified using fluorochrome conjugated aerolysin (FLAER, Pinewood Scientific), a bacterial toxin that specifically binds GPI anchors, and did not show significant differences between the affected individual, the heterozygous individuals, and the controls (data not shown).

Altered GPI anchors are resistant to PI-PLC cleavage

We then investigated the expected structural abnormality of GPI-anchors by testing sensitivity of GPI-APs to phosphatidylinositol-specific phospholipase C (PI-PLC) [31]. The LCLs were incubated with 10 unit/ml of PI-PLC for 1.5 h at 37°C and the remaining surface GPI-APs were determined by flow cytometry. Of GPI-APs, 61% to 90% were removed from the surface of LCLs of the healthy sister with a homozygous wildtype (Figure 3A, solid line) and healthy control individuals (data not shown). In contrast, no significant or only slight reduction of the surface GPI-APs was seen with LCLs from the affected person (Figure 3A), indicating that almost all GPI-APs on the affected LCLs had abnormal GPI anchors resistant to PI-PLC [4]. This is a strong indication that the p.Leu197del mutation causes null or almost null activity of the PGAP1 enzyme. GPI-APs on LCLs from heterozygous parents were only partially sensitive to PI-PLC (Figure 3A), indicating that the p.Leu197del mutation causes haplo-insufficiency. These defective sensitivities of affected the person's and parents' GPI-APs to PI-PLC were fully restored by transfection of wild-type *PGAP1* cDNA (Figure 3B, solid lines).

Finally, the functional effect of the p.Leu197del mutation was tested in the *PGAP1* deficient Chinese hamster ovary (CHO) cell system [4]. GPI-APs expressed on the *PGAP1* deficient CHO cells are resistant to PI-PLC and the activity of *PGAP1* cDNA can be assessed by its ability to make PI-PLC-sensitive GPI-APs after transfection. CHO cells defective for *PGAP1* were transiently transfected with N-terminally-FLAG-tagged wild-type and p.Leu197del mutant human *PGAP1* cDNA in an expression vector with a strong SRα promoter, or an empty vector. Four days after transfection, each transfectant was treated with or without PI-PLC, and the surface expression of CD59, DAF and urokinase plasminogen activator receptor (uPAR) were assessed by flow cytometry. The wild-type *PGAP1* cDNA rescued PI-PLC sensitivity (Figure 4A, left panels). In contrast, the transfection of the mutant p.Leu197del cDNA did not increase the sensitivity to PI-PLC, thus indicating functional loss of the mutant *PGAP1* cDNA (Figure 4A, center panels). To determine PGAP1 protein levels, lysates were prepared two days after transfection, immunoprecipitated with anti-FLAG beads and analyzed by SDS-PAGE/Western blotting. The p.Leu197del mutant protein was not detected at all, indicating that the deletion of Leu197 caused an unstable protein (Figure 4B).

In order to evaluate other known variants in *PGAP1*, we screened the public database of ESP (see above). Of listed variants, we chose the two most frequent variants: rs142320636: c.331A>G (p.Lys111Glu) and rs62185645: c.1753C>G (p.Gln585Glu), and tested the functional effect of these mutations in the *PGAP1* deficient Chinese hamster ovary (CHO) cell system. Transfection of the mutant p.Lys111Glu cDNA did not increase the sensitivity to PI-PLC, indicating functional loss of the mutant *PGAP1* cDNA. Mutant p.Gln585Glu showed an activity comparable to the wild type PGAP1 (Figure S1). Thus, it is possible that homozygosity of p.Lys111Glu leads to ARID.

Discussion

Eight GPI deficiencies caused by hypomorphic mutations in the coding regions of GPI biosynthesis genes *PIGM*, *PIGA*, *PIGL*, *PIGV*, *PIGN*, *PIGO*, *PIGT*, and *PGAP2* have been reported. Except *PIGM*, all lead to a decreased surface expression of GPI-APs and result in intellectual disability, often associated with epilepsy, distinct facial characteristics, and further organ malformations [9–22]. We showed here that complete *PGAP1* deficiency did not affect the surface expression of GPI-APs but expressed structurally abnormal GPI-APs with the acylated inositol.

In previous works, we have reported that *Pgap1* knock-out mice had otocephaly, male infertility, growth retardation, and often died right after birth [32]. Also further two mutant mouse strains, *oto*^{vray} (*oto* for otocephaly) [33,34] and *beaker* [35] were reported to have disrupted *Pgap1*. Both mice strains showed developmental abnormalities of the forebrain; the recessive lethal *oto*^{vray} showed a truncation of the forbrain and the *breaker* mutant displayed a holoprosencephaly-like phenotype. Both Wnt signaling and Nodal signaling were reported to be affected in these mutant mice. These data emphasize the importance of *PGAP1* for vital functions and for brain development. It was also indicated that the *Pgap1* mutant mice phenotypes are dependent upon the genetic background

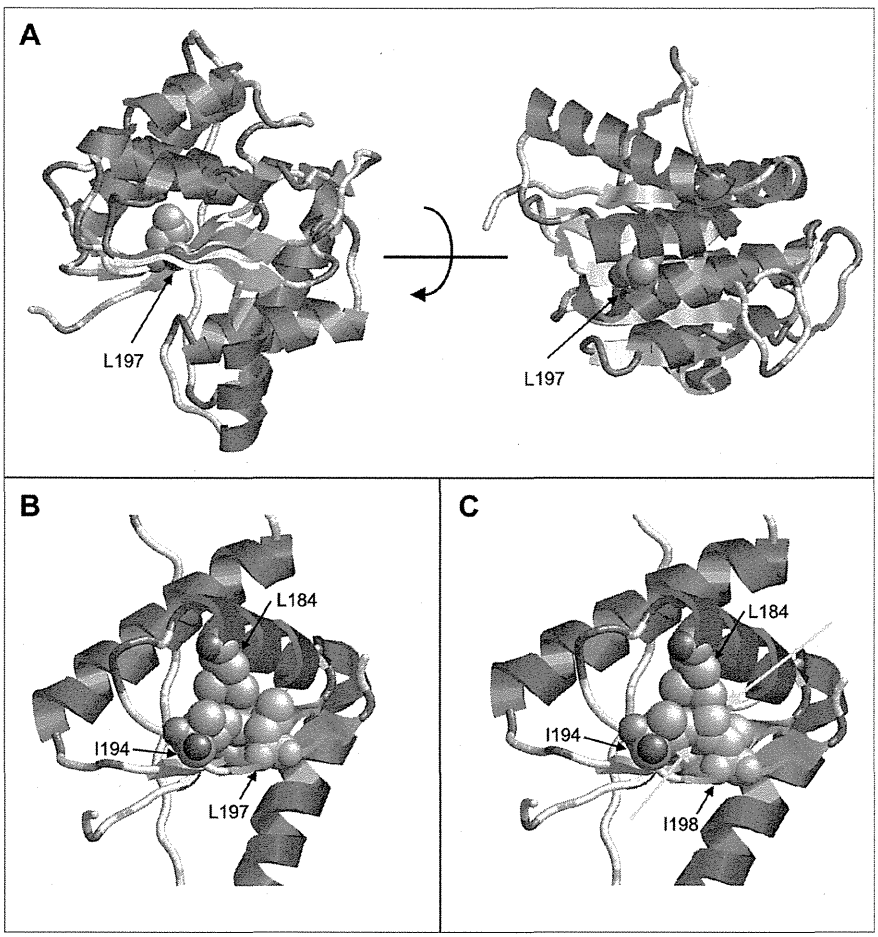

Figure 2. Molecular modeling of PGAP1. (A) Model of PGAP1 highlighting the position of Leu197. The two views differ by a rotation of 90° around the horizontal axis. (B) Interactions of Leu197 (green) with residues Leu184 and Ile194 of the hydrophobic core. (C) Interactions of Ile198 (green) in the Leu197del mutant. Clashes with the adjacent amino acids Leu184 and Ile194 are indicated by cyan arrows. Residues 203–316 are not shown in (B) and (C) for reasons of clarity.
doi:10.1371/journal.pgen.1004320.g002

since otocephaly and holoprosencephaly are not seen in some mouse strains [34,35].

Based on our mapping results, exome sequencing data and functional experiments that proved pathogenicity of the mutation, the previous reports on intellectual disability caused by mutations in the GPI synthesis pathway, and the mouse models that clearly show an association between the disruption of *Pgap1* and abnormalities of brain, we consider the deletion of leucine197 to be causative for the severe non-specific autosomal recessive intellectual disability in our examined patients of family MR079. *PGAP1* is the ninth gene of the GPI synthesis pathway that is now associated to a human phenotype (Table 1). Further mutations in *PGPA1* are needed to confirm our findings. Also, describing further patients with different mutations is necessary to delineate the phenotypes of the GPI deficiencies. For example, considering the defect in the modification of the GPI anchors, the alkaline phosphatase would not be elevated in patients with *PGAP1* mutations, but this needs to be confirmed.

In conclusion, null mutations in *PGAP1* lead to severe intellectual disability and encephalopathy with no obvious malformations; we add *PGAP1* to the growing number of genes involved in GPI-anchor deficiencies with human phenotypes. *PGAP1* deficiency causes a defect in the ER part of the GPI-AP biosynthesis that involves the remodeling of the anchors after attachment to proteins, and it leads to normal protein expression on the cell surface but to abnormal anchor structure.

Materials and Methods

The study was approved by the Ethic Committees of the Universities of Bonn and of Erlangen-Nürnberg in Germany, and Osaka University in Japan. Informed consent of all examined persons or of their guardians was obtained.

Mapping and exome sequencing

Genomic DNA was extracted from EDTA blood probes by standard methods and genotyped with the Affymetrix Mapping array 6.0 (Affymetrix, Santa Clara, CA, USA). Analysis did not reveal pathogenic deletions or duplications. Mendelian segregation was calculated using PedCheck software and was confirmed in all instances. Autozygosity mapping was performed using HomozygositymMapper [36]. DNA from individual III-3 was enriched using the

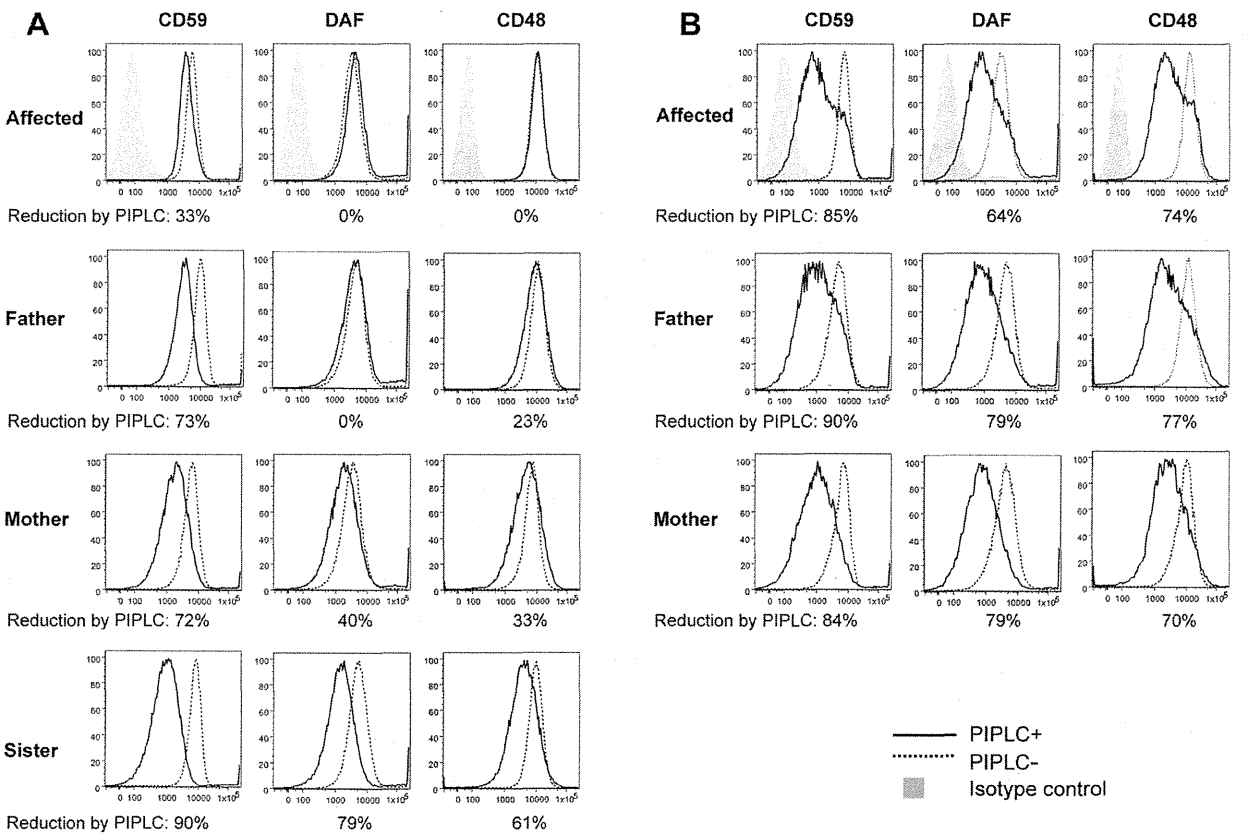

Figure 3. FACS analysis of GPI-APs on LCLs and their PI-PLC sensitivity. (A, B) Cells from one of the affected siblings (III-3) and the parents were transfected with empty pMEoriP vector (A) and pMEoriP-FLAG-humanPGAP1 (B). Cells from the healthy sister were used without transfection. Four days after transfection, cells were treated with (solid lines) or without (dotted lines) 10 unit/ml of PI-PLC for 1.5 h at 37°C, and the surface expression of CD59, DAF and CD48 were assessed by flow cytometry.
doi:10.1371/journal.pgen.1004320.g003

SureSelect Human All Exon Kit, which targets approximately 50 Mb of human genome (Agilent, Santa Clara, Ca, USA) and paired-end sequenced on a SOLiD 5500 xl instrument (Life Sciences, Carlsbad, CA, U.S.A.). Image analysis and base calling was performed using the SOLiD instrument control software with default parameters. Read alignment was performed with LifeScope 2.5 using the default parameters with human genome assembly hg19 (GRCh37) as reference. Single-nucleotide variants and small insertions and deletions (indels) were detected using LifeScope, GATK 2 and samtools/bcftools [37,38]. To replicate the results, DNA from individuals III-2 and III-3 was amplified using the Ion AmpliSeq Exome Kit (Life Technologies, Carlsbad, CA, U.S.A.) which targets approximately 58 Mb of the human genome. After quality control on the Bioanalyzer High Sensitivity Chip (Agilent, Santa Clara, Ca, USA) and emulsion PCR (Ion PI Template OT2 200 Kit v3, Life Technologies, Carlsbad, CA, U.S.A.) the samples were sequenced on a Proton PI chip Version 2 (Life Technologies, Carlsbad, CA, U.S.A.). Base calling, pre-processing of the reads, short read alignment and variant calling was performed using the Torrent Suite including the Torrent Variant Caller (TVC, Version 4.0) with default parameters recommended for the Ampliseq Exome panel (low stringency calling of germline variants, Version September 2013). Variant annotation was performed using Annovar, integrating data from a variety of public databases [39,40]. Additionally, variants were compared to an in-house database containing more than 350 sequenced exomes to identify further common variants which are not present in public databases. Finally, the variants were validated by PCR and Sanger sequencing according to the standard protocols to exclude technical artifacts and to test for segregation.

PI-PLC treatment and FACS analysis

Heparin blood samples were collected from one affected and from all unaffected siblings and parents. Lymphoblastoid Cell lines (LCLs) were generated and cultured in RPMI 1640 (Gibco, Life technologies, Darmstadt, Germany) that is supplemented with 10% FCS (PAA Biotech, Cölbe, Germany) and different other supplements. LCLs from one of the affected siblings (III-3) and the parents were transfected with empty pMEoriP vector or pMEoriP-FLAG-humanPGAP1. Cells from healthy sister were used without transfection. Cells (5×10^6) were suspended in 0.8 ml of Opti-MEM and electroporated with 20 µg each of the plasmids at 260 V and 960 µF using a Gene Pulser (Bio Rad, Hercules, CA). Four days after transfection, cells were treated with or without 10 unit/ml of PI-PLC (Molecular probes, Eugene, OR) for 1.5 h at 37°C. Surface expression of GPI-APs was determined by staining cells with mouse anti-human CD59 (5H8), -human DAF (IA10), -human CD48 (BJ40) antibodies and each isotype IgG followed by a PE-conjugated anti-mouse IgG antibody (BJ40, mouse IgG1 and IgG2a, and secondary antibody were purchased from BD

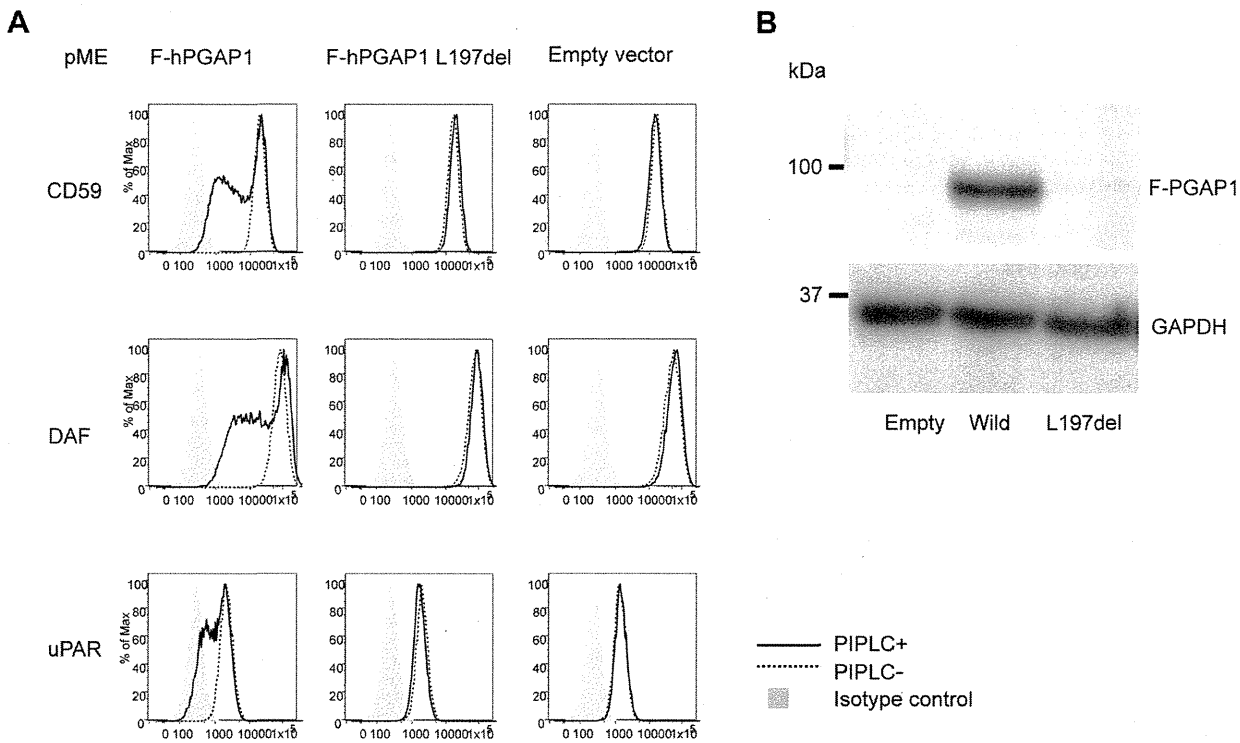

Figure 4. Functional ability of mutant *PGAP1* cDNA. (A) *PGAP1* deficient CHO cell (C10) [4] were transiently transfected with N-terminally-FLAG-tagged wild-type and mutant (L197del) human *PGAP1* driven by a strong promoter SRa, or an empty vector. Four days after transfection, each transfectant was treated with (solid lines) or without (dotted lines) 10 unit/ml of PI-PLC for 1.5 h at 37°C and the surface expression of CD59, DAF and uPAR were assessed by flow cytometry. (B) Two days after transfection of each *PGAP1* construct, lysates were immunoprecipitated with anti-FLAG beads and analyzed by SDS-PAGE/Western blotting. L197del mutant protein was not detected at all.
doi:10.1371/journal.pgen.1004320.g004

Biosciences, Franklin Lakes, NJ) and analyzed by flow cytometer (Cant II; BD Biosciences) using Flowjo software (Tommy Digital Inc., Tokyo, Japan).

Functional analysis using CHO cells

pMEFLAG-hPGAP1 mutant (L197del) bearing patient's mutation was generated by site directed mutagenesis. *PGAP1* deficient CHO cell (C10) [4] were transiently transfected with wild type or mutant pMEFLAG-hPGAP1 by electroporation. Cells (10^7) were suspended in 0.4 ml of Opti-MEM and electroporated with 20 μg each of the plasmids at 260 V and 960 μF using a Gene Pulser. Four days after transfection, cells were treated with or without 10 unit/ml of PI-PLC for 1.5 h at 37°C. Surface expression of GPI-APs was determined by staining cells with mouse anti-human CD59 (5H8), -human DAF (IA10), -hamster uPAR (5D6) antibodies and each isotype IgG, followed by a PE-conjugated anti-mouse IgG antibody and analyzed by flow cytometer using Flowjo software. Two days after transfection of each *PGAP1* construct, lysates were immunoprecipitated with anti-FLAG beads and analyzed by SDS-PAGE/Western blotting.

Web resources

1000Genomes, http://www.1000genomes.org/

ABI, L.T. (2012). LifeScope.: http://www.lifetechnologies.com/lifescope.

ANNOVAR: http://www.openbioinformatics.org/annovar/

GeneTalk: http://www.gene-talk.de

BWA, Burrows-Wheeler Aligner; http://bio-bwa.sourceforge.net/

dbSNP, NCBI: http://www.ncbi.nlm.nih.gov/snp/

GATK 2, Genome Analysis Toolkit: http://www.broadinstitute.org/gatk/index.php

Kyoto Encyclopedia of Genes and Genomes, KEGG, http://www.genome.jp/kegg/

MutationTaster: http://www.mutationtaster.org/ELAND, alignment algorithm, Illumina.com

NHLBI Exome Sequencing Project (ESP): http://evs.gs.washington.edu/EVS/

Online Mendelian Inheritance in Man (OMIM): http://www.omim.org

PolyPhen2: http://genetics.bwh.harvard.edu/pph2/

SIFT: http://sift.jcvi.org/

UCSC Genome Browser: www.genome.ucsc.edu

Supporting Information

Figure S1 Functional ability of mutant *PGAP1* cDNA. *PGAP1* deficient CHO cell (C10) [4] were transiently transfected with N-terminally-FLAG-tagged wild-type and mutant (Lys111Glu, Gln585Glu) human *PGAP1* or an empty vector driven by a strong promoter SRα (pME) or a weak promoter containing only TATA box (pTal). Four days after transfection, each transfectant was treated with (solid lines) or without (dotted lines) 10 unit/ml of PI-PLC for 1.5 h at 37°C and the surface expression of CD59 was assessed by flow cytometry.
(JPG)

Table S1 A list of all ESP database variants with a possible pathogenic effect (i. e. coding or at splice sites). We undertook further in silico analyses using MutationTaster and SIFT and presented in the last two columns estimations about the pathogenicity of the variants. Taking those estimations and the number of identified alleles, one can estimate the prevalence of the disease in the population to be between 7 and 13 per million. (PDF)

Acknowledgments

We are grateful to the families involved in this study for their participation. We thank Karen Toma, Petra Rothe, Heike Friebel-Stange, and Angelika Diem from Erlangen for assistance with LCLs, SNP array genotyping, and NGS. We also thank Mandy Krumbiegel for her support in establishing new NGS methods. We thank Kana Miyanagi from Osaka University for functional analysis.

Author Contributions

Conceived and designed the experiments: YMu AR TK RAJ YMa. Performed the experiments: YMu RB FR HT SS MA HS CB. Analyzed the data: YMu RB FR HT HS RAJ CB. Contributed reagents/materials/analysis tools: SS MA HS YMa. Wrote the paper: YMu TK RAJ.

References

1. Tiede A, Bastisch I, Schubert J, Orlean P, Schmidt RE (1999) Biosynthesis of glycosylphosphatidylinositols in mammalian and unicellular microbes. Biol Chem 380: 503–523.
2. McConville MJ, Menon AK (2000) Recent developments in the cell biology and biochemistry of glycosylphosphatidylinositol lipids. Mol Membr Biol 17: 1–16.
3. Fujita M, Kinoshita T (2012) GPI-anchor remodeling: potential functions of GPI-anchors in intracellular trafficking and membrane dynamics. Biochim Biophys Acta 1821: 1050–1058.
4. Tanaka S, Maeda Y, Tashima Y, Kinoshita T (2004) Inositol deacylation of glycosylphosphatidylinositol-anchored proteins is mediated by mammalian PGAP1 and yeast Bst1p. J Biol Chem 279: 14256–14263.
5. Fujita M, Maeda Y, Ra M, Yamaguchi Y, Taguchi R, et al. (2009) GPI glycan remodeling by PGAP5 regulates transport of GPI-anchored proteins from the ER to the Golgi. Cell 139: 352–365.
6. Tashima Y, Taguchi R, Murata C, Ashida H, Kinoshita T, et al. (2006) PGAP2 is essential for correct processing and stable expression of GPI-anchored proteins. Mol Biol Cell 17: 1410–1420.
7. Maeda Y, Tashima Y, Houjou T, Fujita M, Yoko-o T, et al. (2007) Fatty acid remodeling of GPI-anchored proteins is required for their raft association. Mol Biol Cell 18: 1497–1506.
8. Almeida AM, Murakami Y, Baker A, Maeda Y, Roberts IA, et al. (2007) Targeted therapy for inherited GPI deficiency. N Engl J Med 356: 1641–1647.
9. Johnston JJ, Gropman AL, Sapp JC, Teer JK, Martin JM, et al. (2012) The phenotype of a germline mutation in PIGA: the gene somatically mutated in paroxysmal nocturnal hemoglobinuria. Am J Hum Genet 90: 295–300.
10. van der Crabben SN, Harakalova M, Brilstra EH, van Berkestijn FM, Hofstede FC, et al. (2013) Expanding the spectrum of phenotypes associated with germline PIGA mutations: A child with developmental delay, accelerated linear growth, facial dysmorphisms, elevated alkaline phosphatase, and progressive CNS abnormalities. Am J Med Genet A 164: 29–35.
11. Swoboda KJ, Margraf RL, Carey JC, Zhou H, Newcomb TM, et al. (2013) A novel germline PIGA mutation in Ferro-Cerebro-Cutaneous syndrome: A neurodegenerative X-linked epileptic encephalopathy with systemic iron-overload. Am J Med Genet A 164: 17–28.
12. Krawitz PM, Murakami Y, Hecht J, Kruger U, Holder SE, et al. (2012) Mutations in PIGO, a member of the GPI-anchor-synthesis pathway, cause hyperphosphatasia with mental retardation. Am J Hum Genet 91: 146–151.
13. Krawitz PM, Schweiger MR, Rodelsperger C, Marcelis C, Kolsch U, et al. (2010) Identity-by-descent filtering of exome sequence data identifies PIGV mutations in hyperphosphatasia mental retardation syndrome. Nat Genet 42: 827–829.
14. Horn D, Wieczorek D, Metcalfe K, Baric I, Palezac L, et al. (2013) Delineation of PIGV mutation spectrum and associated phenotypes in hyperphosphatasia with mental retardation syndrome. Eur J Hum Genet doi:10.1038/ejhg.2013.241.
15. Kuki I, Yukitoshi Takahashi, Shin Okazaki, Hisashi Kawawaki, Eiji Ehara, Norimitsu Inoue, Taroh Kinoshita and Yoshiko Murakami (2013) Case report on vitamin B6 responsive epilepsy due to inherited GPI deficiency. Neurology 81: 1467–1469.
16. Nakamura K, Osaka H, Murakami Y, Anzai R, Nishiyama K, et al. (2014) PIGO mutations in intractable epilepsy and severe developmental delay with mild elevation of alkaline phosphatase levels. Epilepsia 55 (2): e13–e17.
17. Maydan G, Noyman I, Har-Zahav A, Neriah ZB, Pasmanik-Chor M, et al. (2011) Multiple congenital anomalies-hypotonia-seizures syndrome is caused by a mutation in PIGN. J Med Genet 48: 383–389.
18. Ohba C, Okamoto N, Murakami Y, Suzuki Y, Tsurusaki Y, et al. (2013) PIGN mutations cause congenital anomalies, developmental delay, hypotonia, epilepsy, and progressive cerebellar atrophy. Neurogenetics doi: 10.1007/s10048-013-0384-7.
19. Ng BG, Hackmann K, Jones MA, Eroshkin AM, He P, et al. (2012) Mutations in the glycosylphosphatidylinositol gene PIGL cause CHIME syndrome. Am J Hum Genet 90: 685–688.
20. Kvarnung M, Nilsson D, Lindstrand A, Korenke GC, Chiang SC, et al. (2013) A novel intellectual disability syndrome caused by GPI anchor deficiency due to homozygous mutations in PIGT. J Med Genet 50: :521–528.
21. Hansen L, Tawamie H, Murakami Y, Mang Y, Ur Rehman S, et al. (2013) Hypomorphic Mutations in PGAP2, Encoding a GPI-Anchor-Remodeling Protein, Cause Autosomal-Recessive Intellectual Disability. Am J Hum Genet 92: 575–583.
22. Krawitz PM, Murakami Y, Riess A, Hietala M, Kruger U, et al. (2013) PGAP2 Mutations, Affecting the GPI-Anchor-Synthesis Pathway, Cause Hyperphosphatasia with Mental Retardation Syndrome. Am J Hum Genet 92: 584–589.
23. Murakami Y, Kanzawa N, Saito K, Krawitz PM, Mundlos S, et al. (2012) Mechanism for release of alkaline phosphatase caused by glycosylphosphatidylinositol deficiency in patients with hyperphosphatasia mental retardation syndrome. J Biol Chem 287: 6318–6325.
24. Abou Jamra R, Wohlfart S, Zweier M, Uebe S, Priebe L, et al. (2011) Homozygosity mapping in 64 Syrian consanguineous families with non-specific intellectual disability reveals 11 novel loci and high heterogeneity. Eur J Hum Genet 19: 1161–1166.
25. Abou Jamra R, Philippe O, Raas-Rothschild A, Eck SH, Graf E, et al. (2011) Adaptor protein complex 4 deficiency causes severe autosomal-recessive intellectual disability, progressive spastic paraplegia, shy character, and short stature. Am J Hum Genet 88: 788–795.
26. Montosi G, Donovan A, Totaro A, Garuti C, Pignatti E, et al. (2001) Autosomal-dominant hemochromatosis is associated with a mutation in the ferroportin (SLC11A3) gene. J Clin Invest 108: 619–623.
27. Njajou OT, Vaessen N, Joosse M, Berghuis B, van Dongen JW, et al. (2001) A mutation in SLC11A3 is associated with autosomal dominant hemochromatosis. Nat Genet 28: 213–214.
28. Kurowski MA, Bujnicki JM (2003) GeneSilico protein structure prediction meta-server. Nucleic Acids Res 31: 3305–3307.
29. Sanchez R, Sali A (2000) Comparative protein structure modeling. Introduction and practical examples with modeller. Methods Mol Biol 143: 97–129.
30. Rauch A, Wieczorek D, Graf E, Wieland T, Endele S, et al. (2012) Range of genetic mutations associated with severe non-syndromic sporadic intellectual disability: an exome sequencing study. Lancet 380: 1674–1682.
31. Volwerk JJ, Shashidhar MS, Kuppe A, Griffith OH (1990) Phosphatidylinositol-specific phospholipase C from Bacillus cereus combines intrinsic phosphotransferase and cyclic phosphodiesterase activities: a 31P NMR study. Biochemistry 29: 8056–8062.
32. Ueda Y, Yamaguchi R, Ikawa M, Okabe M, Morii E, et al. (2007) PGAP1 knock-out mice show otocephaly and male infertility. J Biol Chem 282: 30373–30380.
33. Zoltewicz JS, Plummer NW, Lin MI, Peterson AS (1999) oto is a homeotic locus with a role in anteroposterior development that is partially redundant with Lim1. Development 126: 5085–5095.
34. Zoltewicz JS, Ashique AM, Choe Y, Lee G, Taylor S, et al. (2009) Wnt signaling is regulated by endoplasmic reticulum retention. PLoS One 4: e6191.
35. McKean DM, Niswander L (2012) Defects in GPI biosynthesis perturb Cripto signaling during forebrain development in two new mouse models of holoprosencephaly. Biol Open 1: 874–883.
36. Seelow D, Schuelke M, Hildebrandt F, Nurnberg P (2009) HomozygosityMapper–an interactive approach to homozygosity mapping. Nucleic Acids Res 37: W593–599.
37. McKenna A, Hanna M, Banks E, Sivachenko A, Cibulskis K, et al. (2010) The Genome Analysis Toolkit: a MapReduce framework for analyzing next-generation DNA sequencing data. Genome Res 20: 1297–1303.
38. Li H, Handsaker B, Wysoker A, Fennell T, Ruan J, et al. (2009) The Sequence Alignment/Map format and SAMtools. Bioinformatics 25: 2078–2079.
39. Wang K, Li M, Hakonarson H (2010) ANNOVAR: functional annotation of genetic variants from high-throughput sequencing data. Nucleic Acids Res 38: e164.
40. Abecasis GR, Altshuler D, Auton A, Brooks LD, Durbin RM, et al. (2010) A map of human genome variation from population-scale sequencing. Nature 467: 1061–1073.

Neurogenetics (2014) 15:193–200
DOI 10.1007/s10048-014-0408-y

ORIGINAL ARTICLE

Novel compound heterozygous *PIGT* mutations caused multiple congenital anomalies-hypotonia-seizures syndrome 3

Mitsuko Nakashima · Hirofumi Kashii · Yoshiko Murakami · Mitsuhiro Kato · Yoshinori Tsurusaki · Noriko Miyake · Masaya Kubota · Taroh Kinoshita · Hirotomo Saitsu · Naomichi Matsumoto

Received: 21 February 2014 / Accepted: 25 May 2014 / Published online: 8 June 2014

Abstract Recessive mutations in genes of the glycosylphosphatidylinositol (GPI)-anchor synthesis pathway have been demonstrated as causative of GPI deficiency disorders associated with intellectual disability, seizures, and diverse congenital anomalies. We performed whole exome sequencing in a patient with progressive encephalopathies and multiple dysmorphism with hypophosphatasia and identified novel compound heterozygous mutations, c.250G>T (p. Glu84*) and c.1342C>T (p. Arg488Trp), in *PIGT* encoding a subunit of the GPI transamidase complex. The surface expression of GPI-anchored proteins (GPI-APs) on patient granulocytes was lower than that of healthy controls. Transfection of the Arg488Trp mutant *PIGT* construct, but not the Glu84* mutant, into PIGT-deficient cells partially restored the expression of GPI-APs DAF and CD59. These results indicate that *PIGT* mutations caused neurological impairment and multiple congenital anomalies in this patient.

M. Nakashima · Y. Tsurusaki · N. Miyake · H. Saitsu · N. Matsumoto (✉)
Department of Human Genetics, Yokohama City University Graduate School of Medicine, 3-9 Fukuura, Kanazawa-ku, Yokohama 236-0004, Japan
e-mail: naomat@yokohama-cu.ac.jp

H. Kashii · M. Kubota
Division of Neurology, National Center for Child Health and Development, Tokyo, Japan

Y. Murakami · T. Kinoshita
Research Institute for Microbial Diseases and World Premier International Immunology Frontier Research Center, Osaka University, Osaka, Japan

M. Kato
Department of Pediatrics, Yamagata University Faculty of Medicine, Yamagata, Japan

Keywords Whole exome sequencing · *PIGT* · Compound heterozygous mutations · Glycosylphosphatidylinositol-anchored protein · Multiple congenital anomalies-hypotonia-seizures syndrome 3 · Hypophosphatasia

Introduction

Glycosylphosphatidylinositol (GPI) acts as the anchor of various eukaryotic proteins expressed on the plasma membrane. GPI synthesis and GPI-anchored protein (GPI-AP) modification are mediated by at least 27 genes in the endoplasmic reticulum (ER) and Golgi apparatus [1]. Recent studies have indicated that inherited loss-of-function mutations in these genes lead to GPI deficiencies associated with neurological impairments including seizures, intellectual disability, and multiple congenital anomalies [2–9]. In addition, somatic mutations in PIGA cause paroxysmal nocturnal haemoglobinuria, a haematopoietic disease, which is also caused by somatic mutation of PIGT in combination with the germ line mutation of one allele [10, 11].

PIGT is one of the subunits of the GPI transamidase complex, and catalyzes the attachment of GPI anchors to proteins in the ER [1]. Kvarnung et al. [12] previously reported a homozygous *PIGT* mutation in patients from a consanguineous Turkish family with multiple congenital anomalies-hypotonia-seizures syndrome-3 (MCAHS3 [MIM 615398]). In the present study, we describe the use of whole exome sequencing to identify novel compound heterozygous *PIGT* mutations in a Japanese patient with seizures, intellectual disability and multiple congenital anomalies. Functional analysis indicated that these mutations are causative of GPI deficiency.

Patient and methods

Patient

The female proband was born at full term without asphyxia as the first child of healthy unrelated parents (Fig. 1a). Polyhydramnios was recognized during pregnancy. She showed poor sucking and post-feed stridor soon after birth. At 4 months of age, she showed tonic seizures with apnea and myoclonic seizures, both of which repeatedly turned to convulsive status. Her electroencephalogram (EEG) demonstrated high-amplitude slow wave as a background activity, but no epileptic discharges were observed. She also showed a poor response, muscle hypotonia, unstable head control, a cardiac murmur caused by patent ductus arteriosus, and left hydronephroureter with ureteral stenosis. Her seizures were refractory to multiple antiepileptic drugs such as carbamazepine, clobazam, and an intravenous injection of pyridoxal phosphate while the frequency of her seizures decreased with the combination of valproic acid, zonisamide, and phenytoin to some extent. Phenobarbital could not be used in infancy because of drug eruption. After 1 year of age, she was frequently admitted to hospital because of convulsive status epilepticus induced by fever, or recurrent episodes of respiratory infections, bronchial asthma, or gastroenteritis. Her sleep cycle was disorganized. Brain magnetic resonance imaging at 3 years of age demonstrated progressive atrophy of the cerebral hemisphere, cerebellum, and brainstem (Fig. 1c). EEG at 3 years showed borderline findings consisting of a predominance of fast wave activity with no spindle formation interrupted by slow wave burst. She recurrently suffered bone fractures without obvious event. Systemic bone X-ray at 12 years of age showed neurogenic arthrogryposis and osteoporosis. At 12 years of age, she was bedridden and was only able to roll over. She showed profound intellectual disability and had no meaningful words. Her epileptic seizures disappeared after 10 years of age, but epileptic discharges comprised of spike-and-slow wave complex at bilateral frontal area with low-amplitude irregular background activity were seen on EEG.

G-banded chromosomal analysis revealed a normal karyotype (46,XX). Metabolic screenings including amino acids, lactic acid, pyruvic acid, organic acids, lactic acid, and lysosomal enzymes were unremarkable. The biochemical analysis of blood repeatedly showed low levels of serum alkaline phosphatase from birth (186 U/l at birth and 326 U/l at 7 years of age [normal range, 450–1250 U/l]). Both concentrations of serum and urine calcium were normal (serum calcium, 9.6 mg/dl; U-calcium/U-creatinine ratio, 0.23 at 7 years of age).

DNA preparation

Peripheral blood samples were obtained from the patient and her parents after parents signed informed consent. DNA was extracted using QuickGene-610 L (Fujifilm, Tokyo, Japan) according to the manufacturer's instructions. The study was approved by the ethics committee of the Yokohama City University.

Whole exome sequencing

Patient DNA was captured with the SureSelect Human All Exon V5 Kit (Agilent Technologies, Santa Clara, CA, USA) and sequenced on an Illumina Hiseq2000 (Illumina, San Diego, CA, USA) with 101-bp paired-end reads. Image analysis and base calling were performed by sequence control software real-time analysis and CASAVA software v1.8 (Illumina). Reads were mapped to the human reference genome sequence (UCSC hg19, NCBI build 37) and aligned using Novoalign (Novocraft Technologies, Jaya, Malaysia). PCR duplicate reads were excluded using Picard (http://picard.sourceforge.net/) for further analysis. Single-nucleotide variants (SNVs) and small indels were identified using the Genome Analysis Toolkit UnifiedGenotyper [13] and filtered according to the Broad Institute's best-practice guidelines (version 3). Variants that passed the filters were annotated using ANNOVAR[14]. The damaging prediction was performed by Polyphen-2 [15] and MutationTaster software [16].

Sanger sequencing

PIGT exon 2 and exon 10 sequences were PCR amplified from the patient and her parents using the following primers: *PIGT* ex2F 5′-GGGAGGAACTTGTCATCACC-3′ and ex2R 5′-CAGTGGCAGGATGACAACAC-3′, *PIGT* ex10F 5′-AGAGATGTGGGTGACCTTGC-3′ and ex10R 5′-CTGAGGACAGATGGGCTACA-3′, respectively. Amplified PCR products were sequenced on an ABI 3500xl or 3130xl Genetic Analyzer (Applied Biosystems, Foster City, CA, USA).

Flow cytometry

Peripheral blood samples were collected from the patient and normal control individuals. Granulocyte surface expression of total GPI-APs was quantified by staining with Alexa 488-conjugated inactivated aerolysin (FLAER; Protox Biotech, Victoria, Canada). Expression of CD16, CD24, and alkaline phosphatase (ALP) was examined using appropriate primary antibodies (3G8, ML5, and B4-78, respectively; BD Biosciences, Franklin Lakes, NJ, USA), followed by a PE-conjugated anti-mouse IgG secondary antibody (BD Biosciences). Cells were analyzed by BD FACSCanto II (BD Biosciences).

Human *PIGT* cDNA (NM_015937.5) with FLAG at the C terminus was subcloned into the pME (driven by a strong SRα promoter) or pTA (driven by a weak promoter

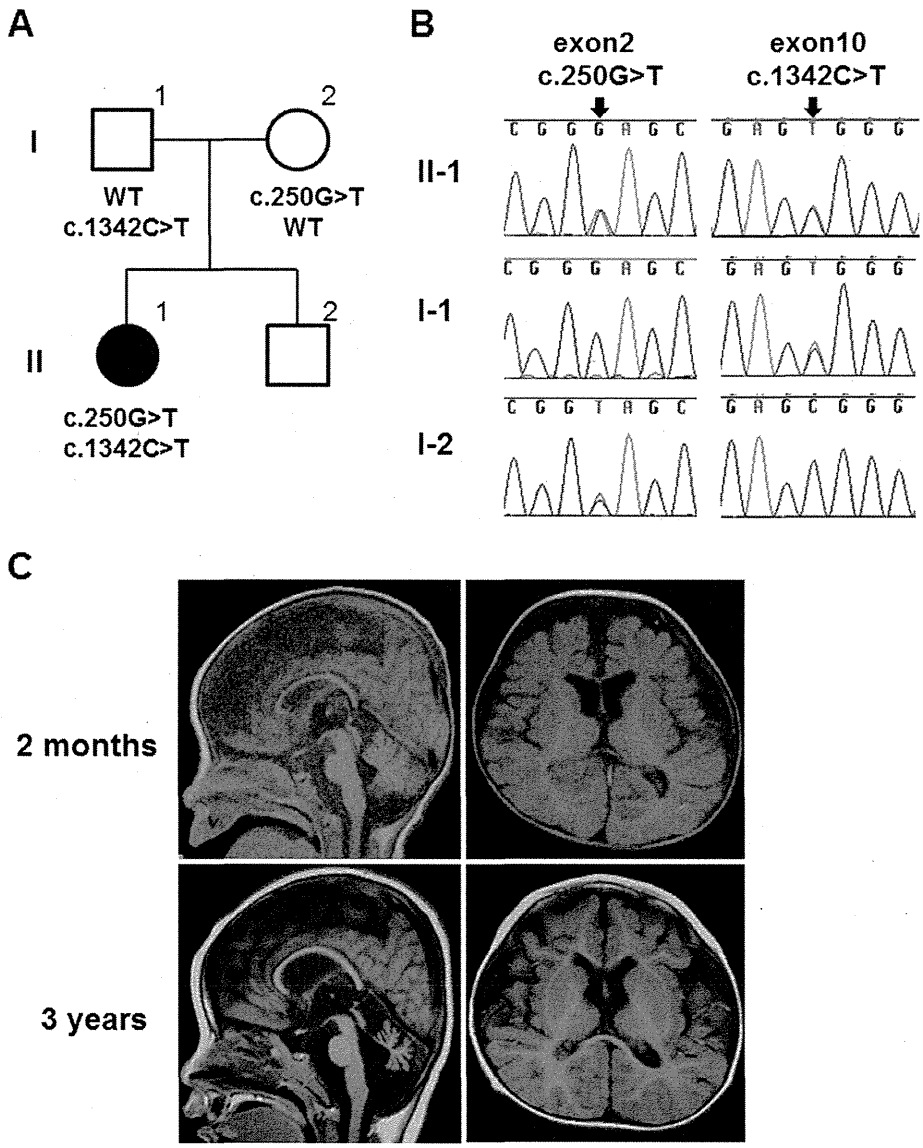

Fig. 1 **a** Familial pedigree. **b** Sanger sequencing results. Compound heterozygous mutations, c.250G>T and c.1342C>T, in *PIGT* were observed in the affected individual. c.250G>T (*left*) and c.1342C>T (*right*) were inherited from the mother and the father, respectively. **c** Magnetic resonance imaging of the patient's brain. Axial and sagittal T1-weighted images at 3 years of age show atrophic changes of the cerebral hemisphere, brainstem, and cerebellum

containing only TATA-box) vector [17]. Two *PIGT* mutants, Glu84* and Arg488Trp, were generated by site-directed mutagenesis. Mutant and wild-type *PIGT* plasmids were transfected by electroporation into CHO H4, *PIGT*-deficient Chinese hamster ovary (CHO) cells expressing human DAF (also called CD55) and CD59 as previously described [18]. Two days later, lysates were run on SDS-PAGE, and Western blotting was performed using an anti-FLAG antibody (M2; Sigma-Aldrich, St. Louis, MO, USA) to detect FLAG-tagged PIGT (PIGT-F). The protein levels were normalized to the loading control, and luciferase activities were used to evaluate transfection efficiencies. Cells were stained with anti-hCD59 (5H8), anti-hDAF (IA10), and anti-Hamster uPAR (5D6) antibodies and restoration of the surface expression of GPI-APs was assessed by flow cytometry.

Results

Mutation screening

We performed mutation screening for previously reported genes involved in the GPI-anchor–synthesis pathway, and identified the compound heterozygous mutations c.250G>T (p. Glu84*) and c.1342C>T (p. Arg488Trp) in *PIGT* (NM_015937.5). Both mutations were not found in 6500

ESP (Exome Sequencing Project) or 1000 genomes [19, 20], but c.1342C>T is present in one of 408 in-house control exomes. Both mutations were predicted to be probably disease-causing by Polyphen-2 and MutationTaster. Sanger sequencing confirmed that c.250G>T and c.1342C>T were inherited from the mother and father, respectively (Fig. 1b).

Functional effect of the mutations on GPI synthesis

PIGT is a component of GPI transamidase that mediates the post-translational attachment of GPI anchors to the C-terminal of the precursor protein. Therefore, the mutant GPI transamidase is likely to impair the surface expression of GPI-APs. To investigate the influence of *PIGT* mutations on GPI-APs synthesis, we first examined the granulocyte surface expression of GPI-APs from the patient and a healthy control. Expression of total GPI-APs (FLAER staining) and GPI-APs CD16 and ALP on granulocytes was reduced in the patient compared to the normal control (Fig. 2a). However, similar expression levels of another GPI-AP CD24 were seen in the patient and control (Fig. 2a).

We then transiently transfected wild-type or mutant (Glu84* or Arg488Trp) *PIGT* cDNA constructs into *PIGT*-deficient CHO cells to evaluate the functional effect of each mutation on GPI-AP expression. Western blotting revealed that the expression level of Arg488Trp mutant protein was similar to that of wild-type protein, whereas the Glu84* mutant expressed a small amount of full-length protein (probably read-though) (Fig. 2c). Wild-type *PIGT* transfection successfully restored the expression of GPI-APs CD59, DAF (CD55), and uPAR in both cases using vectors with a strong (pME) and weak (pTA) promoter (Fig. 2b). The Arg488Trp mutant *PIGT* cloned in pME restored the expression of GPI-APs close to that of wild-type, whereas the same mutant in the pTA vector only partially restored expression. The Glu84* mutant *PIGT* in the pME vector insufficiently restored the expression of GPI-APs, while this mutant in the pTA vector could not restore expression (Fig. 2b). These results demonstrate that both mutants, especially the Glu84* alteration, reduce the activity of PIGT function.

Fig. 2 **a** Surface expression of GPI-APs on granulocytes. Granulocytes from the patient and healthy control were stained with FLAER or antibodies against CD24, CD16, and ALP. The expression of total GPI, CD16, and ALP in the patient (*solid line*) was lower than in the normal control (*dark shaded area*). CD24 expression did not differ between the patient and control. The *light shaded areas* represent the isotype control. *X* axes show fluorescent intensities, which indicate expression levels of each GPI-AP on the cell surface. *Y* axes show the relative cell numbers. The value of mean fluorescent intensities of each sample is shown in each panel. **b** PIGT-deficient CHO cells were transiently transfected with wild-type (*dashed line*), Glu84* mutant (*fine solid line*), or Arg488Trp mutant (*bold solid line*) *PIGT* cDNA expression constructs in vectors with either a strong promoter (pME; *upper panels*) or weak promoter (pTA; *lower panels*). PIGT-F protein levels and restoration of the surface expression of CD59, DAF, and uPAR were assessed 2 days later. The *dark* and *light shadows* represent empty-vector transfectants and isotype controls, respectively. **c** Western blotting showed that the Arg488Trp mutant protein was expressed at similar levels to the wild-type protein, whereas the Glu84* mutant full-length protein, representing the read-through product, was expressed at lower levels. Quantity numbers at the bottom of the gel indicate the relative intensity of PIGT-F protein levels normalized to the loading control, and luciferase activities used for evaluating transfection efficiencies. *Arrowhead* indicates a non-specific product

Discussion

GPI deficiency syndromes are recessive disorders caused by mutations in genes involved in the GPI-anchor biosynthesis pathway. Here, we describe novel compound heterozygous *PIGT* mutations in a nonconsanguineous patient presenting with seizures and intellectual disability.

The first reported *PIGT* mutation (c.547A>C, p.Thr183Pro) was identified in a consanguineous Turkish family who showed seizures, intellectual disability, and multiple congenital anomalies [12]. A decreased expression of GPI-APs was documented on patient granulocytes. They confirmed that the homozygous c.547A>C mutation impaired the function of PIGT by the functional study using *pigt* knockdown zebrafish embryos which showed gastrulation defects phenotype. In the present study, we also demonstrated that both *PIGT* mutations, c.250G>T (p. Glu84*) and c.1342C>T (p. Arg488Trp), impaired the function of PIGT which was confirmed by the functional study using the PIGT deficient CHO cells.

Mammalian GPI transamidase consists of at least five subunits, PIGK, GPAA1, PIGS, PIGT, and PIGU [1]. Of these, PIGT plays a critical role in stabilizing the complex formation of GPI transamidase [17], which mediates cleavage of the GPI attachment signal peptide at the C-terminal of the precursor protein and transfers GPI anchors to the C-terminal of cleaved proteins [1]. Consequently, PIGT mutants may not be able to correctly form the GPI transamidase complex, leading to a loss of GPI transamidase activity and reduction in the cellular surface expression of GPI-APs.

Our patient and four patients described by Kvarnung et al. [12] showed broad clinical spectrum and shared several common features (Table 1). The neurological findings including intractable seizures, hypotonia and severe intellectual disability were observed in all patients. Ophthalmologic features including strabismus, nystagmus, and cerebral visual impairment were also observed in all. Cerebral and cerebellar atrophy was observed in our patient and two of four seen by Kvarnung et al. The EEG findings in our patient were also exacerbated as she grew, suggesting progressive encephalopathy. Our patient and three of four patients by Kvarnung et al. had some cardiologic disorders. All patients had some

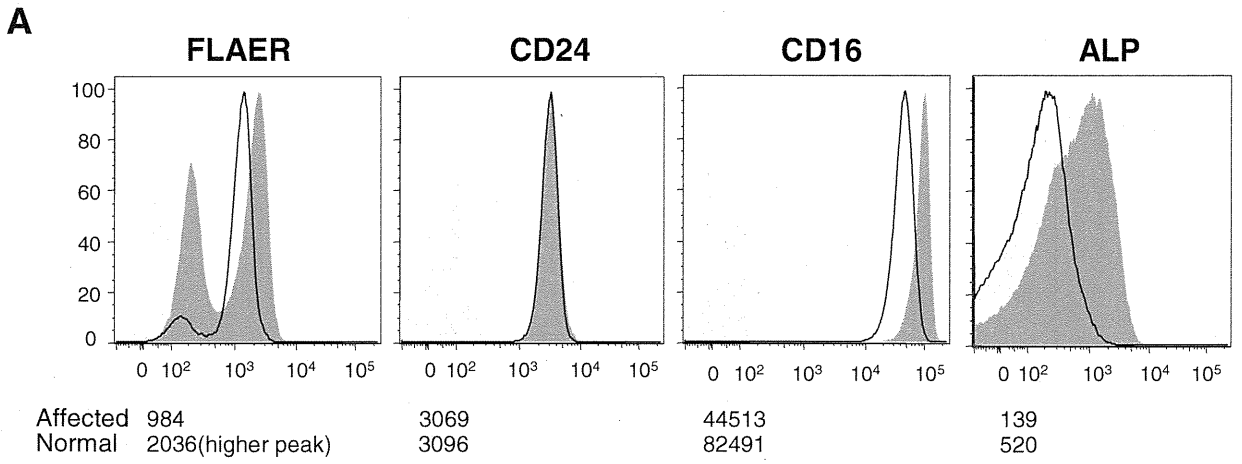
A
FLAER
CD24
CD16
ALP
Affected 984 3069 44513 139
Normal 2036(higher peak) 3096 82491 520

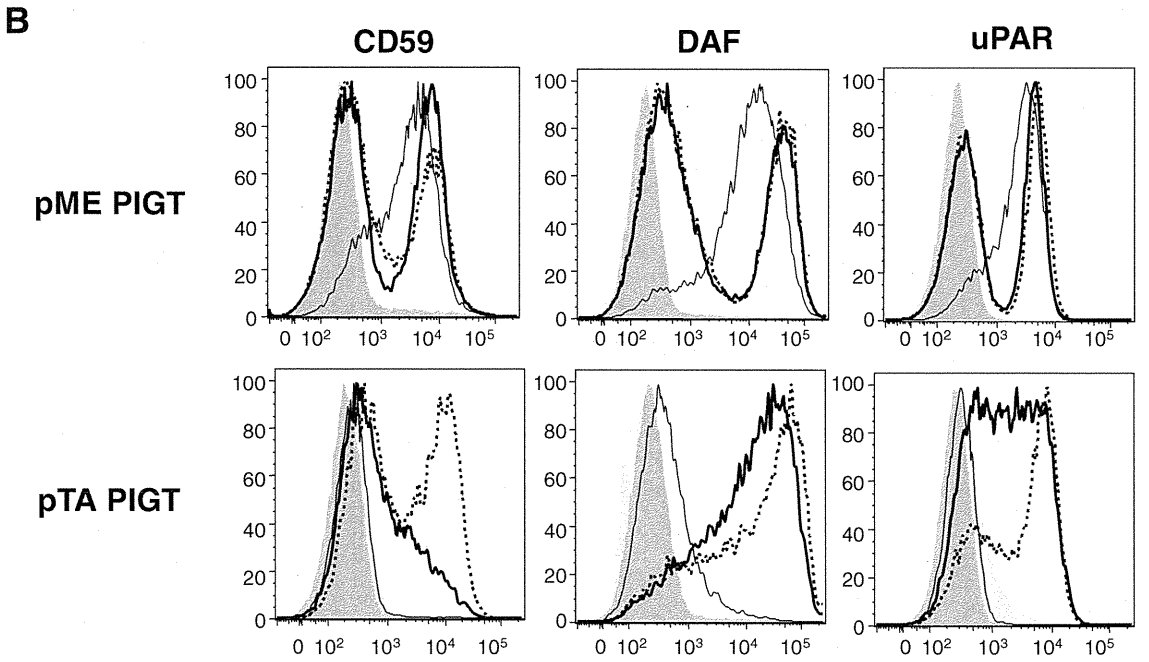
B
CD59
DAF
uPAR
pME PIGT
pTA PIGT

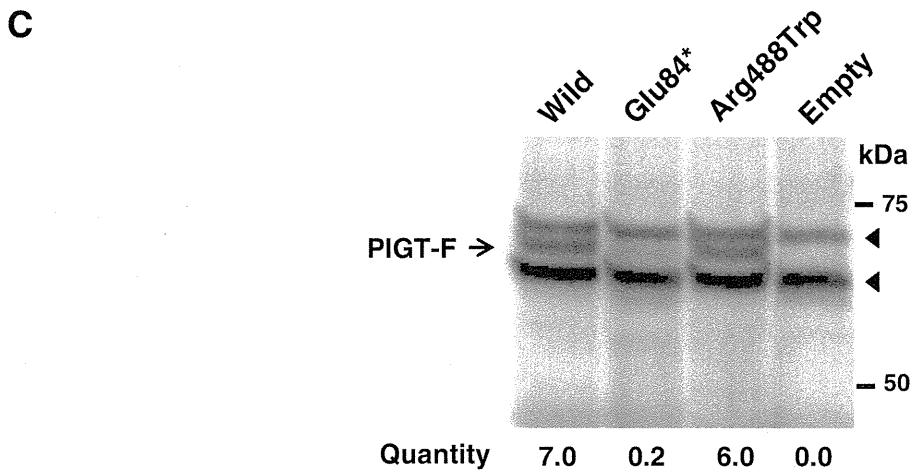
C
Wild
Glu84*
Arg488Trp
Empty
kDa
75
50
PIGT-F
Quantity 7.0 0.2 6.0 0.0

Table 1 Clinical features of patients with PIGT mutations

Patients	This Patient	Kvarnung et al. Patient 1	Kvarnung et al. Patient 2	Kvarnung et al. Patient 3	Kvarnung et al. Patient 4
consanguinity	–	+	+	+	+
Sex	Female	Female	Female	Female	Female
Gestation	40 weeks	40 weeks	39 weeks	37 weeks	37 weeks
Birth weight	3,816 g	4,735 g	4,500 g	3,460 g	3,240 g
Birth length	51 cm	53 cm	54 cm	53 cm	53 cm
BHC	35.5 cm +1.8 SD	38 cm +2 SD	39 cm +3 SD	35 cm +1 SD	36 cm +1.5 SD
HPP	+	+	+	+	+
ID	+	+	+	+	+
Hypotonia	+	+	+	+	+
Seizure	+	+	+	+	+
Strabismus	+	+	+	+	+
Nystagmus	+	+	+	+	+
CVI	+	+	+	+	+
Brain images	CT: dilated ventricle, frontal atrophy, cerebellar and brainstem atrophy	CT: primitive Sylvian fissures	CT: Normal findings	MRI: global atrophy with predominate vermis and cerebellar atrophy, atrophy of basal ganglia	MRI: global atrophy with predominat vermis and cerebellar atrophy, hypomyelination
Tooth abnormalities	–	+	+	+	+
Skeletal features	Scoliosis, osteoporosis	Craniosynostosis, Pectus excavatum, Short arm, Scoliosis, Delayed bone age, Reduced mineralisation	Craniosynostosis, short arm, Scoliosis, Delayed bone age, Reduced mineralisation	Short arm, Delayed bone age, Reduced mineralisation	Short arm, Delayed bone age, Reduced mineralisation
Urologic features	Urolithiasis, Ureteral dilation	Nephrocalcinosis	Nephrocalcinosis, Ureteral dilation, Cysts and dysplasia	Nephrocalcinosis, Ureteral dilation	Nephrocalcinosis, Ureteral dilation
Cardiologic features	PDA	Minor PDA	–	Mild restrictive CMP	Increased atrial load on ECG
Facial features	Low set ears, micrognathia, malar flattening, upslanting palpebral fissures, depressed nasal bridge, short anteverted nose, downturned corners of the mouth, tented lip, high arched palate	High forehead with bitemporal narrowing, broad nasal root, anteverted nose, long philtrum with a deep groove, distinct cupid bow	High forehead with bitemporal narrowing, broad nasal root, anteverted nose, long philtrum with a deep groove, distinct cupid bow	High forehead with bitemporal narrowing, broad nasal root, anteverted nose, long philtrum with a deep groove, distinct cupid bow	High forehead with bitemporal narrowing, broad nasal root, anteverted nose, long philtrum with a deep groove, distinct cupid bow

BHC birth head circumference, *HPP* hypophosphatasia, *ID* intellectual disability, *CVI* cerebral visual impairment, *ECG* electrocardiogram, *CMP* cardiomyopathy, *PDA* patent ductus arteriosus

urologic features, but not nephrocalcinosis in our patient. Our case shared similar facial features with previous patients including a depressed nasal bridge, short anteverted nose, tented lip, and downturned corners of the mouth. Low set ears, micrognathia, malar flattening, and upslanting palpebral fissures were unique to our patient.

Hyperphosphatasia is a characteristic symptom of some GPI deficiencies, such as PIGV, PIGW, PIGO, PGAP2 and PGAP3 deficiencies [2–6]. In contrast, hypophosphatasia is a particularly distinctive feature in the loss of GPI transamidase function. Murakami at al. suggested that GPI transamidase abnormalities lead to an inability to hydrolyze the precursor protein of alkaline phosphatase, resulting in the degradation of most precursor proteins within the cell and a decrease of serum alkaline phosphatase levels (hypophosphatasia) [21]. This is supported in our case by the hypophosphatasia. The patients described by Kvarnung et al. showed hypercalcemia and hypercalciuria following tooth abnormality, craniosynostosis, a delayed bone age, and reduced mineralization, which is the common features with infantile hypophosphatasia caused by the mutations in *ALPL*, the gene encoding tissue non-specific alkaline phosphatase (TNAP) [22]. As TNAP is a GPI-AP, the PIGT deficiency causes decreased surface expression of TNAP, which would lead to bone abnormalities. Regardless of hypophosphatasia, our case showed only mild scoliosis and osteoporosis, but no tooth abnormality nor craniosynostosis. Different mutational effects on the enzyme activity may account for such different phenotypes. In this study, mutant PIGT construct harboring Arg488Trp or Glu84* in strong promoter (pME) vector restored GPI-Aps expression. In contrast, Kvarnung et al. showed that abnormal phenotype of pigt knockdown zebrafish was never restored by the homozygous mutant (Thr183Pro) PIGT cDNA. Therefore, it is possible to estimate that the Thr183Pro mutation may affect the GPI transamidase complex activity more severely than the Arg488Trp and Glu84* mutations, leading to less severe phenotypes. However, further functional analysis and cases with *PIGT* mutations are needed to elucidate the relevance of these mutations in PIGT function and full clinical spectrum of GPI deficiency syndromes.

Acknowledgments We thank the patient's family for participating in this work. We also thank Nobuko Watanabe for her technical assistance. This study was supported by the Ministry of Health, Labour and Welfare of Japan, a Grant-in-Aid for Scientific Research (A), (B), and (C) from the Japan Society for the Promotion of Science, the Takeda Science Foundation, the fund for Creation of Innovation Centers for Advanced Interdisciplinary Research Areas Program in the Project for Developing Innovation Systems, the Strategic Research Program for Brain Sciences, and a Grant-in-Aid for Scientific Research on Innovative Areas (Transcription Cycle) from the Ministry of Education, Culture, Sports, Science and Technology of Japan.

Conflict of interest The authors declare that they have no conflict of interest.

References

1. Kinoshita T, Fujita M, Maeda Y (2008) Biosynthesis, remodelling and functions of mammalian GPI-anchored proteins: recent progress. J Biochem 144(3):287–294. doi:10.1093/jb/mvn090
2. Krawitz PM, Schweiger MR, Rodelsperger C, Marcelis C, Kolsch U, Meisel C, Stephani F, Kinoshita T, Murakami Y, Bauer S, Isau M, Fischer A, Dahl A, Kerick M, Hecht J, Kohler S, Jager M, Grunhagen J, de Condor BJ, Doelken S, Brunner HG, Meinecke P, Passarge E, Thompson MD, Cole DE, Horn D, Roscioli T, Mundlos S, Robinson PN (2010) Identity-by-descent filtering of exome sequence data identifies PIGV mutations in hyperphosphatasia mental retardation syndrome. Nat Genet 42(10):827–829. doi:10.1038/ng.653
3. Krawitz PM, Murakami Y, Hecht J, Kruger U, Holder SE, Mortier GR, Delle Chiaie B, De Baere E, Thompson MD, Roscioli T, Kielbasa S, Kinoshita T, Mundlos S, Robinson PN, Horn D (2012) Mutations in PIGO, a member of the GPI-anchor-synthesis pathway, cause hyperphosphatasia with mental retardation. Am J Hum Genet 91(1):146–151. doi:10.1016/j.ajhg.2012.05.004
4. Hansen L, Tawamie H, Murakami Y, Mang Y, ur Rehman S, Buchert R, Schaffer S, Muhammad S, Bak M, Nothen MM, Bennett EP, Maeda Y, Aigner M, Reis A, Kinoshita T, Tommerup N, Baig SM, Abou Jamra R (2013) Hypomorphic mutations in PGAP2, encoding a GPI-anchor-remodeling protein, cause autosomal-recessive intellectual disability. Am J Hum Genet 92(4):575–583. doi:10.1016/j.ajhg.2013.03.008
5. Howard MF, Murakami Y, Pagnamenta AT, Daumer-Haas C, Fischer B, Hecht J, Keays DA, Knight SJ, Kolsch U, Kruger U, Leiz S, Maeda Y, Mitchell D, Mundlos S, Phillips JA 3rd, Robinson PN, Kini U, Taylor JC, Horn D, Kinoshita T, Krawitz PM (2014) Mutations in PGAP3 impair GPI-anchor maturation, causing a subtype of hyperphosphatasia with mental retardation. Am J Hum Genet 94(2):278–287. doi:10.1016/j.ajhg.2013.12.012
6. Chiyonobu T, Inoue N, Morimoto M, Kinoshita T, Murakami Y (2013) Glycosylphosphatidylinositol (GPI) anchor deficiency caused by mutations in PIGW is associated with West syndrome and hyperphosphatasia with mental retardation syndrome. J Med Genet. doi:10.1136/jmedgenet-2013-102156
7. Krawitz PM, Murakami Y, Riess A, Hietala M, Kruger U, Zhu N, Kinoshita T, Mundlos S, Hecht J, Robinson PN, Horn D (2013) PGAP2 mutations, affecting the GPI-anchor-synthesis pathway, cause hyperphosphatasia with mental retardation syndrome. Am J Hum Genet 92(4):584–589. doi:10.1016/j.ajhg.2013.03.011
8. Almeida AM, Murakami Y, Layton DM, Hillmen P, Sellick GS, Maeda Y, Richards S, Patterson S, Kotsianidis I, Mollica L, Crawford DH, Baker A, Ferguson M, Roberts I, Houlston R, Kinoshita T, Karadimitris A (2006) Hypomorphic promoter mutation in PIGM causes inherited glycosylphosphatidylinositol deficiency. Nat Med 12(7):846–851. doi:10.1038/nm1410
9. Ng BG, Hackmann K, Jones MA, Eroshkin AM, He P, Wiliams R, Bhide S, Cantagrel V, Gleeson JG, Paller AS, Schnur RE, Tinschert S, Zunich J, Hegde MR, Freeze HH (2012) Mutations in the glycosylphosphatidylinositol gene PIGL cause CHIME syndrome. Am J Hum Genet 90(4):685–688. doi:10.1016/j.ajhg.2012.02.010
10. Johnston JJ, Gropman AL, Sapp JC, Teer JK, Martin JM, Liu CF, Yuan X, Ye Z, Cheng L, Brodsky RA, Biesecker LG (2012) The phenotype of a germline mutation in PIGA: the gene somatically mutated in paroxysmal nocturnal hemoglobinuria. Am J Hum Genet 90(2):295–300. doi:10.1016/j.ajhg.2011.11.031
11. Krawitz PM, Hochsmann B, Murakami Y, Teubner B, Kruger U, Klopocki E, Neitzel H, Hoellein A, Schneider C, Parkhomchuk D, Hecht J, Robinson PN, Mundlos S, Kinoshita T, Schrezenmeier H (2013) A case of paroxysmal nocturnal hemoglobinuria caused by a

germline mutation and a somatic mutation in PIGT. Blood 122(7): 1312–1315. doi:10.1182/blood-2013-01-481499
12. Kvarnung M, Nilsson D, Lindstrand A, Korenke GC, Chiang SC, Blennow E, Bergmann M, Stodberg T, Makitie O, Anderlid BM, Bryceson YT, Nordenskjold M, Nordgren A (2013) A novel intellectual disability syndrome caused by GPI anchor deficiency due to homozygous mutations in PIGT. J Med Genet 50(8):521–528. doi:10.1136/jmedgenet-2013-101654
13. DePristo MA, Banks E, Poplin R, Garimella KV, Maguire JR, Hartl C, Philippakis AA, del Angel G, Rivas MA, Hanna M, McKenna A, Fennell TJ, Kernytsky AM, Sivachenko AY, Cibulskis K, Gabriel SB, Altshuler D, Daly MJ (2011) A framework for variation discovery and genotyping using next-generation DNA sequencing data. Nat Genet 43(5):491–498. doi:10.1038/ng.806
14. Wang K, Li M, Hakonarson H (2010) ANNOVAR: functional annotation of genetic variants from high-throughput sequencing data. Nucleic Acids Res 38(16):e164. doi:10.1093/nar/gkq603
15. Adzhubei IA, Schmidt S, Peshkin L, Ramensky VE, Gerasimova A, Bork P, Kondrashov AS, Sunyaev SR (2010) A method and server for predicting damaging missense mutations. Nat Methods 7(4):248–249. doi:10.1038/nmeth0410-248
16. Schwarz JM, Rodelsperger C, Schuelke M, Seelow D (2010) MutationTaster evaluates disease-causing potential of sequence alterations. Nat Methods 7(8):575–576. doi:10.1038/nmeth0810-575
17. Ohishi K, Inoue N, Kinoshita T (2001) PIG-S and PIG-T, essential for GPI anchor attachment to proteins, form a complex with GAA1 and GPI8. EMBO J 20(15):4088–4098. doi:10.1093/emboj/20.15.4088
18. Ashida H, Hong Y, Murakami Y, Shishioh N, Sugimoto N, Kim YU, Maeda Y, Kinoshita T (2005) Mammalian PIG-X and yeast Pbn1p are the essential components of glycosylphosphatidylinositol-mannosyltransferase I. Mol Biol Cell 16(3):1439–1448. doi:10.1091/mbc.E04-09-0802
19. Genomes Project C, Abecasis GR, Altshuler D, Auton A, Brooks LD, Durbin RM, Gibbs RA, Hurles ME, McVean GA (2010) A map of human genome variation from population-scale sequencing. Nature 467(7319):1061–1073. doi:10.1038/nature09534
20. Genomes Project C, Abecasis GR, Auton A, Brooks LD, DePristo MA, Durbin RM, Handsaker RE, Kang HM, Marth GT, McVean GA (2012) An integrated map of genetic variation from 1,092 human genomes. Nature 491(7422):56–65. doi:10.1038/nature11632
21. Murakami Y, Kanzawa N, Saito K, Krawitz PM, Mundlos S, Robinson PN, Karadimitris A, Maeda Y, Kinoshita T (2012) Mechanism for release of alkaline phosphatase caused by glycosylphosphatidylinositol deficiency in patients with hyperphosphatasia mental retardation syndrome. J Biol Chem 287(9):6318–6325. doi:10.1074/jbc.M111.331090
22. Mornet E (2007) Hypophosphatasia. Orphanet J Rare Dis 2:40. doi:10.1186/1750-1172-2-40

EUROPEAN JOURNAL OF Haematology

European Journal of Haematology 92 (450–453)

CASE REPORT

Paroxysmal nocturnal hemoglobinuria with copy number-neutral 6pLOH in GPI (+) but not in GPI (−) granulocytes

Yasutaka Ueda[1], Jun-ichi Nishimura[2], Yoshiko Murakami[3,4], Sachiko Kajigaya[1], Taroh Kinoshita[3,4], Yuzuru Kanakura[2], Neal S. Young[1]

[1]Hematology Branch, National Heart, Lung, and Blood Institute, National Institutes of Health, Bethesda, MD, USA; [2]Department of Hematology and Oncology, Osaka University Graduate School of Medicine, Osaka; [3]Department of Immunoregulation, Research Institute for Microbial Diseases, Osaka University, Osaka; [4]Department of Immunoglycobiology, WPI Immunology Frontier Research Centre, Osaka University, Osaka, Japan

Abstract

Paroxysmal nocturnal hemoglobinuria (PNH) is an acquired bone marrow disorder caused by expansion of a clone of hematopoietic cells lacking glycosylphosphatidylinositol (GPI)-anchored membrane proteins. Multiple lines of evidence suggest immune attack on normal hematopoietic stem cells provides a selective growth advantage to PNH clones. Recently, frequent loss of HLA alleles associated with copy number-neutral loss of heterozygosity in chromosome 6p (CN-6pLOH) in aplastic anemia (AA) patients was reported, suggesting that AA hematopoiesis 'escaped' from immune attack by loss of HLA alleles. We report here the first case of CN-6pLOH in a Japanese PNH patient only in GPI-anchored protein positive (59%) granulocytes, but not in GPI-anchored protein negative (41%) granulocytes. CN-6pLOH resulted in loss of the alleles *A*02:06-DRB1*15:01-DQB1*06:02*, which have been reported to be dominant in Japanese PNH patients. Our patient had maintained nearly normal blood count for several years. Our case supports the hypothesis that a hostile immune environment drives selection of resistant hematopoietic cell clones and indicates that clonal evolution may occur also in normal phenotype (non-PNH) cells in some cases.

Key words paroxysmal nocturnal hemoglobinuria; array comparative genomic hybridization; loss of heterozygosity; clonal evolution; bone marrow failure syndromes

Correspondence Yasutaka Ueda, Hematology Branch, NHLBI/NIH, Bldg 10-CRC, Rm 3E-5216, 9000 Rockville Pike, Bethesda, MD 20892, USA. Tel: 301-451-7132; Fax: 301-496-8396; e-mail: ueday2@nhlbi.nih.gov

Accepted for publication 15 December 2013 doi:10.1111/ejh.12253

Paroxysmal nocturnal hemoglobinuria (PNH) is a rare, life-threatening bone marrow failure syndrome, which is characterized by three major features: intravascular hemolytic anemia, bone marrow failure, and thrombosis (1). PNH is an acquired clonal disorder of the hematopoietic stem cell (HSC) caused by a somatic mutation of the X-linked phosphatidylinositol glycan class A (*PIGA*) gene in one or a few hematopoietic stem cells (2). Even healthy individuals were reported to have very small number of PNH cells (3). The mechanism of clonal expansion of PNH cells is not understood, but the close association between PNH and aplastic anemia (AA) suggests that immune-mediated attack to hematopoietic stem cells underlies the pathogenesis of the association. Some data support a model of PNH clone expansion based on autoimmunity. PNH clones were less sensitive to NK and T-cell killing due to lack of expression of stress-inducible GPI-anchored proteins ULBP1 and ULBP2 in vitro and with patients granulocytes (4, 5), and an inefficient T lymphocyte response was observed to GPI (−) cells *in vitro* and in mouse models (6). Recently, frequent loss of HLA alleles associated with copy number-neutral loss of heterozygosity of the 6p arms (CN-6pLOH) in AA patients was reported (7). Here, we describe the first case of a PNH patient with CN-6pLOH in GPI (+) granulocytes, but not in GPI (−) granulocytes.

Patient and methods

A 33-year-old male presented to hospital for mild thrombocytopenia (130×10^9/L), and PNH was diagnosed by flow

cytometry (1). The patient had not been treated for 2 years and 6 months due to lack of symptoms of anemia or thrombosis, although he had experienced hemoglobinuria several times a year since diagnosis. PNH clone sizes were 49.0% and 22.0% in granulocytes and red blood cells, respectively, at diagnosis and were 45.2% and 28.5%, respectively, 12 months after the diagnosis. LDH had remained elevated (500–600 U/L). At the time of array comparative genomic hybridization (aCGH) analysis, 24 months after the diagnosis, the proportions of GPI-negative cells were 40.9%, 25.7%, and 4.7% in granulocytes, red blood cells, and T cells, respectively. Blood count included leukocytes 3.7×10^9/L, (38.8% neutrophils, 48.0% lymphocytes, 8.7% monocytes, 0.8% eosinophils, and 0.5% basophils), hemoglobin 14.4 g/dL, MCV 101.9 fl, platelets 113×10^9/L, and reticulocyte count 112×10^9/L. LDH was elevated at 620 U/L (normal range up to 229 U/L). Informed consent was obtained from the patient in accordance with protocols approved by the Institutional Review Boards of Osaka University Hospital. Red blood cells were analyzed for GPI-anchored proteins with anti-CD55 and anti-CD59 antibodies within a CD235 positive population. Peripheral blood granulocytes (CD11b + 7AAD−) and T cells (CD3 + 7AAD−) were separated into GPI (+) and GPI (−) cells by Flaer (Pinewood Scientific Services, Victoria, BC, Canada) staining. After sorting, each cell population of granulocytes was subjected to DNA extraction with the QIAamp DNA Blood Mini kit or the QIAamp DNA Micro kit (QIAGEN, Hilden, Germany). High-resolution genome-wide DNA copy number analysis was performed with both GPI (+) and GPI (−) granulocytes using the CytoScan®HD Array (Affymetrix, Santa Clara, CA, USA). Sample processing was performed at Coriell Genotyping and Microarray Center, Coriell Institute for Medical Research (Camden, NJ, USA). Data were analyzed with Affymetrix Chromosome Analysis Suite (CHAS). For the analysis of clonal lesions, loss of heterozygosity (LOH) was called when the deletion was more than 25 Mb and involved telomeres (8). Alleles at *HLA-A*, *-B*, *-DRB1*, *-DQB1*, and *-DPB1* loci were identified by PCR and sequence-specific oligonucleotide probes (PCR-SSOP) method using the WAKFlow HLA Typing kit (Wakunaga, Hiroshima, Japan) at the HLA Foundation Laboratory (Kyoto, Japan), as described previously (9). Briefly, target DNA was PCR amplified with 5′-biotin-labeled primers that are highly specific to sequences of HLA genes. Amplified DNA was denatured and hybridized to locus-specific probes conjugated to microbeads labeled with streptavidin–phycoerythrin. The fluorescent intensity of phycoerythrin on each coded oligobead was measured by the Luminex® 100 system (Luminex, Austin, TX, USA). The data analysis was performed using the WAKFlow® Typing Software (Wakunaga). The haplotypes of six loci were inferred based on the data of haplotype frequencies of a Japanese population (701 families; $n = 2972$) estimated by direct counting method. The data are available at the Web site of the HLA Foundation Laboratory (http://hla.or.jp/haplo/haplonavi.php?type=haplo&lang=en).

Results and discussion

The Affymetrix CytoScan® HD Array contains more than 2.4 million markers for copy numbers and 750 thousand single nucleotide polymorphisms, enabling detection of high-resolution copy number, LOH detection, and breakpoint estimation across the genome. We employed the CytoScan®HD Array for aCGH analysis of submicroscopic aberrations of genomes in three Japanese PNH patients who had both GPI (+) and GPI (−) cells in granulocytes. Remarkably, CN-6pLOH was detected in a GPI (+) granulocyte population, but not in a GPI (−) granulocyte popula-

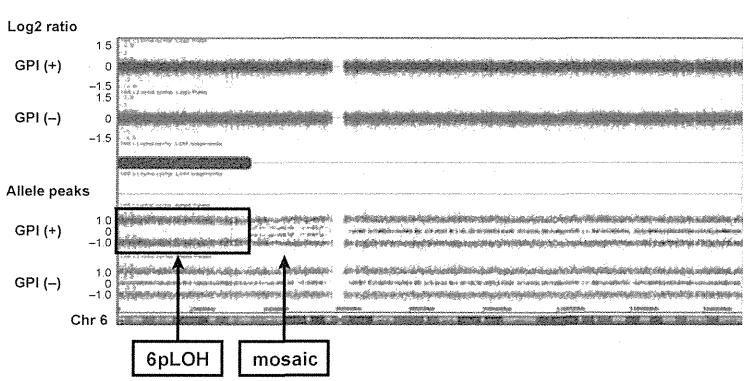

Figure 1 Acquired CN-6pLOH in GPI (+) granulocytes but not in GPI (−) granulocytes. Upper panel shows copy number status by log2 ratio: Theoretically, the log 2 ratio of normal (copy number-neutral) clones is log2 (2/2) = 0 and of single copy losses is log2 (1/2) = −1. Lower panel shows allele frequency calculated as the difference between the signals of the A allele minus B allele. Homozygous AA maps to approximately +1, and homozygous BB allele maps to approximately −1, with the heterozygote mapping to approximately 0. Single A and B allele maps to 0.5 and −0.5, respectively. Copy number was neutral in 6p arm, but loss of heterozygosity (the disappearance of the heterozygote signal) was observed with mosaicism near the centromere.